Pol. J. Environ. Stud. Vol. XX, No. X (XXXX), 1-23
DOI: *10.15244/pjoes/220218* ONLINE PUBLICATION DATE: 2026-07-28

Original Research

Distribution Characteristics and Source Apportionment of Polycyclic Aromatic Hydrocarbons and Sterols in Centennial Sediments of Haizhou Bay

Dong Mu[1], Zhihai Tan[1, 2]*, Longjiang Mao[3], Hao Lei[1], Chenhao Xi[1], Jihong Miao[1], Juan Li[1]

[1]School of Environment and Chemistry Engineering, Xi'an Polytechnic University, China
[2]State Key Laboratory of Loess and Quaternary Geology, Key Laboratory of Aerosol Chemistry and Physics, Institute of Earth Environment, Chinese Academy of Sciences, China
[3]School of Marine Sciences, Nanjing University of Information Science & Technology, Nanjing, Jiangsu 210044, China

Received: 01 February 2026
Accepted: 31 March 2026

Abstract

Haizhou Bay (Jiangsu, eastern China) is a major land-sea transition zone, yet long-term sedimentary records of organic contaminants and their anthropogenic drivers remain poorly constrained, limiting a process-based understanding of regional pollution trajectories and their links to shifts in the energy mix. We quantified 16 priority polycyclic aromatic hydrocarbons (PAHs) and four sterols in four intertidal sediment cores using GC–MS. Spatial variability was evaluated across all cores, whereas centennial-scale (~150-year) temporal changes were interpreted primarily from the representative core HZ02, based on its published ^{210}Pbex–^{137}Cs chronology, for which PAH diagnostic ratios were also assessed. Source patterns were further constrained using bivariate correlations together with principal component analysis and hierarchical clustering. PAH concentrations decreased seaward, whereas sterols were strongly enriched near the Linhong River estuary. In the dated HZ02 record, low-molecular-weight PAHs dominated before 1950, followed by episodic increases in high-molecular-weight PAHs and sterols during the 1950s-1960s and the 1980s-1990s, and a decline in sterols in the early 2000s, consistent with reduced domestic wastewater-related inputs. Multivariate fingerprints indicate two dominant mixed sources: local inputs linked to agricultural biomass burning and household sewage, and an industrial–transport component associated with coal and petroleum combustion and traffic emissions. Contaminant histories covary with population density and energy consumption, supporting a transition from a pre-1950 biomass–sewage-dominated regime to a post-1950 industrial-transport mixture. These century-scale records provide a baseline for

*e-mail: tonishtan@163.com
Tel.: +86-135-7247-3924

reconstructing coastal pollution histories and for evaluating how changes in energy use and emission controls shape organic contamination in eastern China.

Keywords: Haizhou Bay, PAHs, sterols, spatiotemporal patterns, source apportionment

Introduction

Human activities now dominate many Earth-system processes, leaving stratigraphic signals that underpin the proposed Anthropocene [1, 2]. Along rapidly urbanizing coasts, intensified land use and industrial expansion have increased the delivery of terrestrial contaminants to nearshore waters, aggravating eutrophication and ecological stress [3]. By accumulating these contaminants over time, sediments archive the history of human activities while integrating regional environmental change [4-6]. Accordingly, sedimentary geochemical records – among the most integrative and temporally continuous evidence in coastal systems – provide a basis for constraining the magnitude and composition of terrestrial pollutant loading and for evaluating its long-term ecological consequences under Anthropocene conditions.

In coastal sedimentary settings, polycyclic aromatic hydrocarbons (PAHs), sterols, and heavy metals (HMs) are of particular concern because they arise from diverse sources, undergo complex transport and fate processes, and can pose substantial ecological risks [7-9]. PAHs originate primarily from incomplete combustion of fossil fuels and biomass and from petroleum releases; their persistence and strong hydrophobicity favor particle association and long-term accumulation in sediments [10-12]. Sterols are hydrophobic compounds with a strong affinity for organic particles and are well preserved, enabling their long-term retention in sediments and soils [13-15]. Among them, coprostanol is a widely used molecular tracer of human fecal inputs [16, 17]. HMs are largely derived from industrial emissions, coal combustion, traffic, and agricultural activities, and their environmental behavior is influenced by adsorption-desorption and remobilization at the water–sediment interface [18-20]. Riverine discharge, wastewater inputs, and atmospheric deposition jointly deliver organic and inorganic contaminants to coastal depocenters, producing co-enrichment patterns that can track shifts in energy use and regulation over decadal to centennial timescales [21-23]. Sustained atmospheric deposition and land-derived inputs jointly drive the co-accumulation of organic and inorganic contaminants in sediments, highlighting coupled evolutionary pathways of regional mixed pollution [24, 25].

Since the twentieth century, researchers in Europe and North America have pioneered the use of sediment archives to reconstruct pollution histories, demonstrating the profound imprint of human activities on depositional environments [26, 27]. Studies of urban sediments across Europe attribute PAH burdens largely to traffic emissions and coal combustion [28]. In the Langat River (Malaysia), sterol ratios indicate pervasive human fecal inputs, underscoring the influence of population-derived discharges on sediment quality [29]. Further analyses show pronounced co-occurrence of PAHs and the metals Cu and Zn in sediments from the Port of Åland, consistent with the accumulation of mixed contamination driven by shipping activities and antifouling paint use [30]. In a sediment core from Pozzuoli Bay (Italy), PAHs and metal concentrations increased in parallel during the mid-twentieth-century industrial peak and declined thereafter with deindustrialization, highlighting coordinated dynamics of organic and inorganic contaminants during industrial development [31]. Such mixed contaminant signals are increasingly recognized as sensitive geochemical indicators of socioeconomic intensity [24]. Over the past century, sediment-core archives have also captured how contaminant burdens track shifts in energy use and environmental regulation. Records from the U.S. Great Lakes show marked increases in PAHs and metals such as Pb, Zn, and Cu during mid-century industrial expansion, followed by declines after emission controls introduced in the 1970s, reflecting the combined influence of changing fuel structures and policy interventions [26]. In the St. Lawrence Estuary (Canada), PAH inventories are reported to be governed largely by atmospheric deposition and to respond sensitively to variations in human activity [32]. Sediment-core studies from Brazil and the Sea of Japan further indicate that sterols provide stable molecular markers for diagnosing human-waste inputs and shifts in primary production [33, 34]. Together, these continuous archives show that co-enrichment of multiple contaminants can reflect historical changes in human activity, energy use, and regulatory regimes.

In contrast, despite substantial progress in the past two decades, coastal studies in China have largely focused on present-day contamination status and spatial patterns in surface sediments. Work in Bohai Bay and the Chanba River basin documents spatial co-accumulation of PAHs and metals, consistent with mixed inputs from coal combustion, traffic emissions, and biomass burning [35, 36]. In Haizhou Bay and adjacent areas, Cd, Pb, and Zn show pronounced enrichment, with pollution indices increasing alongside intensifying industrial activity [37]. Evidence also points to sustained accumulation of both organic and metal contaminants [38], while PAHs are attributed mainly to road dust, vehicle emissions, petroleum-related inputs, and biomass combustion [39]. However, for China's coastal

waters, understanding of the long-term depositional behavior and historical trajectories of representative organic contaminants remains limited. In particular, there is a shortage of century-scale sediment sequences that can continuously resolve environmental change, which constrains robust reconstruction of accumulation pathways and limits mechanistic insight into how contaminant trends are coupled to regional shifts in energy structure.

Haizhou Bay, a representative semi-enclosed embayment in northern Jiangsu, receives multi-source inputs from port–industrial complexes, energy-production bases, urban effluent, and intensive agriculture. It therefore functions as a major sink for land-derived contaminants and a strategic site for assessing how coastal mixed-contaminant pressures respond to regional energy transitions [40]. Recent studies indicate that the Haizhou Bay ecosystem remains under sustained chemical stress, evidenced by accumulating organic pollutants, enrichment of heavy metals, and elevated ecological risk [41, 42].

Using a high-resolution sediment sequence spanning ~150 years from Haizhou Bay, this study combines quantitative geochemical measurements with multivariate statistics to resolve co-enrichment patterns and century-scale trajectories of PAHs, sterols, and heavy metals. Correlation analysis, hierarchical clustering, and principal component analysis are used to differentiate major sources and pathways of mixed contaminant inputs. By aligning the sedimentary record with the regional history of energy consumption and socioeconomic development, we further evaluate how shifts in energy structure are reflected in the evolving contaminant assemblage. The results constrain the relative contributions of industrialization, urbanization, and agricultural activity to the accumulation of organic and inorganic contaminants in the bay and delineate their spatiotemporal evolution. The novelty of this study lies in three aspects: (i) it provides an age-constrained, centennial-scale sediment record that resolves phase-dependent changes in contaminant concentrations and molecular composition; (ii) it integrates combustion-related PAH metrics with sterol tracers of sewage/terrestrial organic-matter inputs within a unified analytical framework to distinguish source–pathway variability of mixed contamination; and (iii) it interprets these changes in the context of regional energy-use and socioeconomic transitions, thereby offering a testable basis for understanding long-term contaminant trajectories. By integrating multiple independent indicators, this study develops a coherent evidence chain for the long-term evolution of mixed contamination in Haizhou Bay, offering a historical baseline to inform coastal pollution management and evaluations of energy-structure transitions.

Materials and Methods

Study Area

Haizhou Bay (34°30′-35°08′N, 119°23′-119°51′E) is a semi-enclosed embayment on the western Yellow Sea (Lianyungang, Jiangsu, China). The bay covers ~876 km², has a mean depth of ~4.2 m, and reaches ~12 m at its deepest point. It lies at the transition between the Sulu Uplift and the South Yellow Sea Depression. The coastline comprises three geomorphic sectors: (i) an erosional sandy coast in the north (influenced by the Xinzhuang River estuary), (ii) an accretionary silty-mud tidal flat in the central bay, and (iii) a rocky coast in the south (near the Xishu–Shaoxiang River system). This geomorphic heterogeneity modulates sediment dynamics and is expected to shape the spatial distribution of sediment-associated contaminants.

The region has a warm-temperate monsoonal climate (13-14ºC mean annual temperature; ~900-1000 mm annual precipitation, mainly from June to September). Native vegetation is dominated by temperate deciduous broadleaf forest and coastal halophytes, but land use has been extensively modified by human activities. The surrounding area is largely agricultural, with widespread salt pans and aquaculture, whereas urban and industrial land is concentrated along river corridors and the coastal zone. The Qingkou and Linhong rivers are the main tributaries discharging to the bay; the Linhong River receives flow from the Xinmu River and multiple tributaries, delivering substantial loads of nutrients, organic matter, and contaminants and serving as the primary pathway for terrestrial inputs.

The Qingkou River catchment occupies the northern bay, where agriculture and rural settlements are dense, and coal-based energy use, fisheries processing, and shipping are intensive [43]. Qingkou Fishing Port and the adjacent marine ranching area are designated as a provincial fisheries functional zone; however, small coal-fired facilities and shipbuilding/repair activities persist along the shoreline, providing sustained PAH emissions. Together with weak hydrodynamics over the northern muddy tidal flats, these conditions favor contaminant deposition and accumulation [37, 44]. In the south, the Linhong River estuary lies adjacent to the Lianyungang urban area and port hinterland, where an industrial belt dominated by chemicals, construction materials, and energy processing has developed. Urban expansion and the growth of aquaculture have been accompanied by marked increases in domestic sewage and aquaculture effluents [45]. Since 2000, the Linhong River estuary has been incorporated into the “Jiangsu Linhong River Estuary Provincial Wetland Park”, where wetland restoration and wastewater-treatment programs have been implemented [46], leading to a partial reduction in pollutant concentrations discharged to coastal waters.

Sample Collection and Age Dating

To capture spatial heterogeneity in depositional settings, four intertidal sediment-core sites (HZ01-HZ04) were established across Haizhou Bay. HZ01 was located in the upper intertidal zone and was primarily wave-influenced. HZ02 was situated in the river–sea confluence area, where contaminated deposits were most evident. HZ03 and HZ04 were positioned in the lower intertidal zone, representing a more dispersed depositional environment (Fig. 1). Cores were collected using a stainless-steel piston corer (8 cm i.d.) and sectioned at 2 cm intervals, yielding 230 subsamples. Site positions were recorded by GPS (horizontal uncertainty <3 m). All samples were sealed and stored at low temperature prior to analysis.

The age-depth relationship for core HZ02 was adopted from [47], who established a ^{210}Pbex–^{137}Cs chronology for Haizhou Bay (Table 1; Fig. 2). PAHs and sterols were analyzed at the same depth intervals, and the published chronology was used to assign approximate ages to individual layers. As radionuclide dating was not repeated in the present study, temporal variations are interpreted at a decadal scale. The remaining cores (HZ01, HZ03, and HZ04) are therefore discussed primarily in terms of spatial patterns rather than independent age models.

Extraction and Detection

PAHs were extracted and cleaned up using U.S. EPA methods [48], with minor adaptations. Briefly, ~1.5 g of freeze-dried sediment was Soxhlet-extracted with 150 mL acetone-dichloromethane (1:1, v/v). The extract was purified on a 10 g silica-gel column, rinsed with 40 mL n-hexane, and eluted with 20 mL dichloromethane-hexane (1:1, v/v). After concentration to <0.5 mL under gentle N_2, PAHs were analyzed by gas

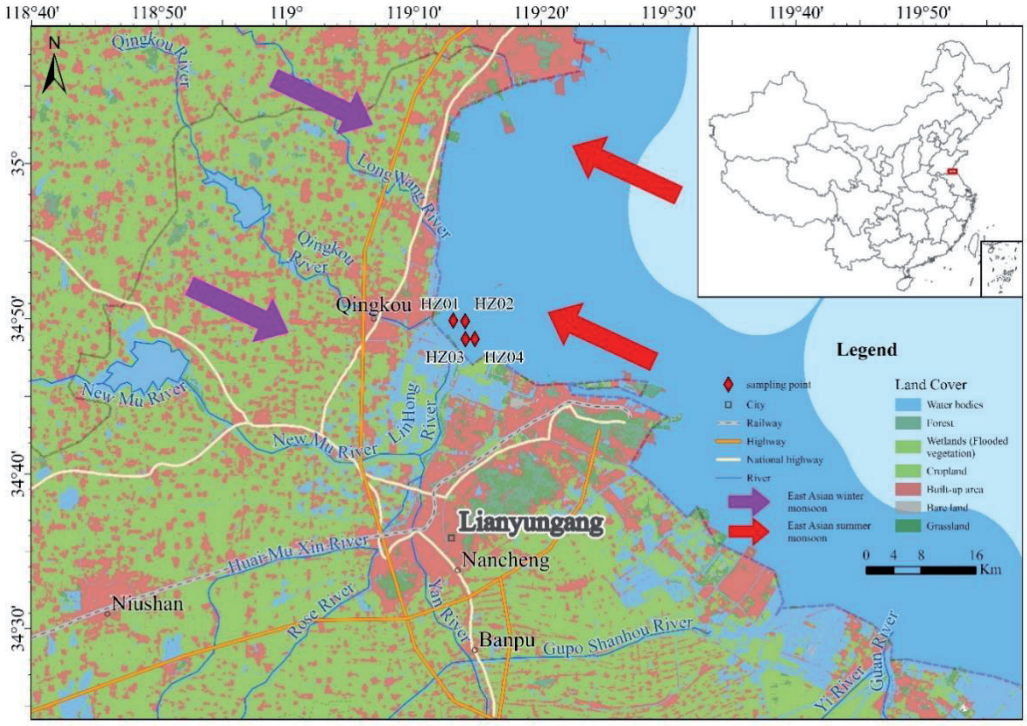

Fig. 1. Location of the sediment-core sampling sites in Haizhou Bay (western Yellow Sea, China). Red diamonds denote core locations (HZ01-HZ04). Purple and red arrows schematically indicate the prevailing wind directions of the East Asian winter monsoon and East Asian summer monsoon, respectively. The inset map shows the position of the study area within China.

Table 1. Cs time markers and derived sedimentation rates for core HZ02.

Time marker	Assigned year	Depth (cm)	Time interval	Sedimentation rate (cm yr^{-1})	Source
^{137}Cs peak	1963	52	1963–2014	1.02	[47]
^{137}Cs peak	1974	46	1974–2014	1.15	[47]
^{137}Cs peak	1986	20	1986–2014	0.71	[47]

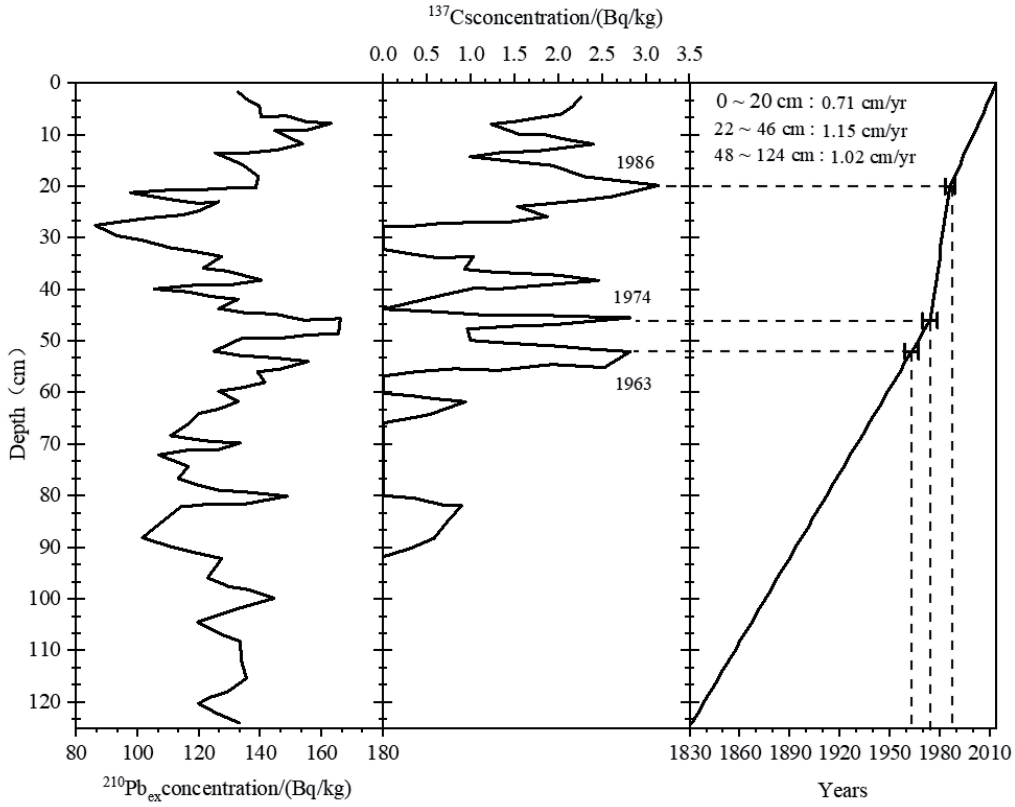

Fig. 2. Profiles of ^{137}Cs and $^{210}Pb_{ex}$ activities and the age–depth relationship for core HZ02 [47]. The chronology was adopted as a temporal reference in this study.

chromatography–mass spectrometry (GC–MS) (Agilent 6890 GC–5975 MS) equipped with an HP-5MS column (30 m × 0.25 mm × 0.25 μm) using helium as carrier gas. The oven program was 100ºC (1 min), 5ºC min^{-1} to 240ºC (20 min), then 10ºC min^{-1} to 280ºC (2 min). Samples (1.5 μL) were injected in splitless mode.

PAHs were determined in selected-ion monitoring (SIM) mode. Target compounds were identified by matching retention times and characteristic ions to those of standards analyzed under the same conditions; the retention times, quantifier ions, and qualifier ions used for confirmation are summarized in Table 2. Quantification was performed using external calibration with an EPA PAH standard mixture (Sigma-Aldrich), and calibration performance was verified every ten samples. Method recoveries ranged from 78.1% to 112.5%.

Sterols were extracted following [49]. Approximately 3 g of oven-dried, sieved sediment (<200 mesh) was ultrasonically extracted with 20 mL dichloromethane–methanol (3:1, v/v) for 30 min. After nitrogen evaporation, the residue was saponified with 1 mL KOH in 10 mL methanol at 80ºC for 4 h. The neutral fraction was isolated by solid-phase extraction (SPE) on a silica-gel cartridge (1 g Na_2SO_4 over 3 g silica gel), preconditioned with 10 mL n-hexane. Eluates were concentrated to ~1.5 mL and derivatized with 200 μL BSTFA + 1% TMCS at 25ºC for 12 h prior to GC–MS analysis (Agilent 6890N GC–5975 MS; HP-5 column, 30 m × 0.25 mm × 0.25 μm) in selected-ion monitoring mode (SIM; m/z 215). Calibration employed coprostanol (COP), epicoprostanol (ECOP), cholesterol (CHOE), and cholestanol (CHOA), with verification every ten samples; recoveries were 79.9%-109.4%.

To interpret the spatiotemporal variability of contaminants and their links to socioeconomic factors, we compiled trace-metal concentration data for the Haizhou Bay sediment core (including As, Ni, Pb, and Zn) and used the published $^{210}Pbex$–^{137}Cs chronological framework to align the metal record with the PAH and sterol profiles at identical (or depth-matched) intervals (nearest-depth matching was applied when necessary). Analytical procedures and quality-control information for metal determination (including As) are compiled [47]. The aligned metal profiles were then used as auxiliary inorganic tracers in correlation analysis, hierarchical clustering, and principal component analysis to evaluate coupled organic-inorganic contamination patterns. City-level indicators for Lianyungang (1950-2015; port throughput; industrial and agricultural output; energy consumption; cultivated land area; population density) were obtained from the Lianyungang Statistical Yearbook [43].

Spatial interpolation and mapping were conducted in ArcGIS 10.8. Correlation analysis, hierarchical cluster analysis (HCA), and principal component analysis (PCA)

Table 2. GC–MS (SIM) parameters for the 16 target PAHs, including retention times and characteristic ions used for quantification and confirmation.

No.	Compound	Retention time (min)	Quantifier ion (m/z)	Qualifier ions (m/z)
1	Naphthalene (Nap)	8.046	128	127, 129
2	Acenaphthylene (Acy)	14.041	152	151, 153
3	Acenaphthene (Ace)	14.859	154	153, 152
4	Fluorene (Flu)	17.096	166	165, 167
5	Phenanthrene (Phe)	21.420	178	179, 176
6	Anthracene (Ant)	21.616	178	179, 176
7	Fluoranthene (Fla)	27.023	202	200, 203, 101, 100
8	Pyrene (Pyr)	27.970	202	200, 203, 101, 100
9	Benzo[a]anthracene (BaA)	35.197	228	226, 229, 114, 113
10	Chrysene (Chr)	35.522	228	226, 229, 114, 113
11	Benzo[b]fluoranthene (BbF)	48.020	252	253, 250, 251
12	Benzo[k]fluoranthene (BkF)	48.247	252	253, 250, 251
13	Benzo[a]pyrene (BaP)	51.691	252	253, 250, 251
14	Indeno[1,2,3-cd]pyrene (IcdP)	60.286	276	277, 275, 274
15	Dibenzo[a,h]anthracene (DahA)	62.448	278	276, 279, 138
16	Benzo[g,h,i]perylene (BghiP)	60.790	276	275, 274, 138

were performed for the dated representative core HZ02 to explore co-variation patterns among PAHs, sterols, and heavy metals and to infer potential controlling sources and processes. In addition, PAH diagnostic ratios (Ant/(Ant+Phe), Fla/(Fla+Pyr), BaA/(BaA+Chry), and IcdP/(IcdP+BghiP)); where Ant = anthracene, Phe = phenanthrene, Fla = fluoranthene, Pyr = pyrene, BaA = benzo[a]anthracene, Chry = chrysene, IcdP = indeno[1,2,3-cd]pyrene, and BghiP = benzo[ghi] perylene) and a fecal sterol index (FSI = COP/(COP+CHOA)) were calculated for HZ02 as supporting source fingerprints.

Temporal variations in Σ_{16}PAHs (sum of 16 priority PAHs), 3-4-ring PAHs, 5-6-ring PAHs, and $\Sigma_4$sterols (sum of COP, ECOP, CHOE, and CHOA) in HZ02 were further compared with regional socioeconomic indicators (energy consumption, port throughput, industrial and agricultural output, cultivated land area, and population density), as well as As as an auxiliary combustion-related tracer. All statistical analyses and visualizations were conducted using SPSS 25 and Origin 2021, and spatial visualization was performed in ArcGIS 10.8.

Results

Over the past ~150 years, all 16 PAHs were detected in the four sediment cores (HZ01-HZ04) from Haizhou Bay. Across the four cores, Σ_{16}PAHs concentrations ranged from 8.614 to 40.48 μg·g^{-1}. Concentrations were higher in HZ01 (12.89-33.38 μg·g^{-1}) and HZ02 (14.38-40.48 μg·g^{-1}) than in HZ03 (9.140-25.80 μg·g^{-1}) and HZ04 (8.614-23.00 μg·g^{-1}) (Fig. 3). At the compound level, Nap varied comparatively little among cores, whereas Phe/Ant/Fla were elevated in HZ02 and BbF/BghiP were enriched in HZ01-HZ02 (Fig. 3). Low-ring PAHs accounted for 15-57% of Σ_{16}PAHs across HZ01-HZ04, whereas high-ring PAHs contributed 14-58%; HZ01 and HZ02 were dominated by 4-6-ring PAHs, while HZ03 and HZ04 were mainly composed of 3-5-ring PAHs (Fig. 3).

Depth profiles reveal pronounced downcore variability in both PAH concentrations and composition (Fig. 4b) and c)). In HZ01 and HZ02, Σ_{16}PAHs and ring-group PAHs display multi-peak patterns along the cores, with relatively higher concentrations in the mid-to-upper sections than in deeper layers (Fig. 4b)). In HZ03 and HZ04, Σ_{16}PAHs also varies substantially with depth (Fig. 4b)). Consistent with the compositional profiles, high-ring PAHs (4-6 rings) increase in relative contribution toward the upper sections of the cores, whereas low-ring PAHs (2-3 rings) contribute more prominently in deeper sections (Fig. 4c)). Across time intervals, PAHs exhibited distinct phases (Fig. 4a)). Before 1950, PAHs showed short-lived peaks dominated by low-ring compounds, whereas high-ring PAHs varied little. From 1950 to 1970, all PAH groups increased markedly, with the strongest rise in 5-6-ring PAHs. During 1980-2000, low-ring PAHs remained relatively

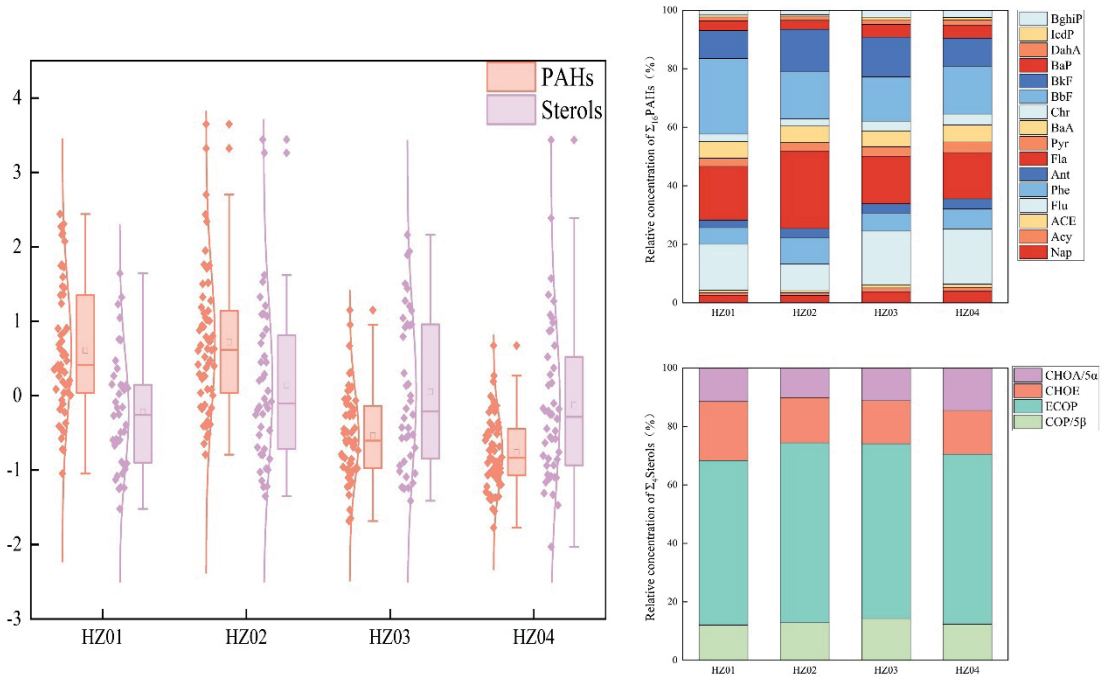

Fig. 3. Spatial contrasts in the standardized levels and compositional fingerprints of PAHs and sterols in four Haizhou Bay sediment cores (HZ01–HZ04). a) Distribution of standardized (z-score) concentrations of Σ_{16}PAHs and Σ_4Sterols in each core (points show individual samples; boxes indicate the median and interquartile range; whiskers denote 1.5×interquartile range (IQR)); b) relative composition of the 16 priority PAHs (percentage contribution to Σ_{16}PAHs) for each core; c) relative composition of sterols (percentage contribution to Σ_4Sterols) for each core.

stable, while 5-6-ring PAHs reached their maximum. Since the early twenty-first century, concentrations of all groups have declined gradually.

Over the past ~150 years, four sterols were detected in all sediment cores from Haizhou Bay. Across HZ01–HZ04, Σ_4 sterol concentrations ranged from 2.971 to 31.89 μg·g^{-1}, with lower concentrations in HZ01 (2.971-21.41 μg·g^{-1}) and HZ02 (3.962-31.89 μg·g^{-1}) but higher concentrations in HZ03 (3.597-24.43 μg·g^{-1}) and HZ04 (3.251-31.85 μg·g^{-1}) (Fig. 3). Σ_4 sterols exhibited phased variability, with a marked increase from the mid-twentieth century and a subsequent decline since the early twenty-first century (Fig. 4). Cholesterol and cholestanol showed only minor variability, whereas fecal sterols (coprostanol and epicoprostanol) increased markedly from the mid-twentieth century onwards. Fecal sterols were ubiquitous in Haizhou Bay sediments, with concentrations ranging from 2.106 to 25.33 μg·g^{-1}. Age-resolved profiles show short-lived peaks before 1950, during 1950-1970, and again in 1980-2000, followed by a gradual decline since the early twenty-first century (Fig. 4).

Pearson correlation analysis (Table 3; Fig. 5a)) indicates a significant positive relationship between Σ_{16}PAHs and sterols (COP, ECOP, CHOA, and CHOE; $r = 0.44$, $p<0.001$). In addition, 4-6-ring PAHs show significant positive correlations with As and with sterols ($p<0.001$).

Hierarchical clustering of the dated HZ02 record (Fig. 5b) and c)) indicates two major groupings during the 1850-1950 interval: Group I comprises mainly 3-ring PAHs together with COP+ECOP, whereas Group II is dominated by 4-6-ring PAHs. After 1950, the clustering structure reorganizes: all PAH homologues (3-6 rings) group together, while COP+ECOP forms a distinct branch (Fig. 5c)).

Principal component analysis (PCA) of the dated representative core HZ02 extracted two principal components explaining 59.9% of the total variance (PC1 = 41.4%, PC2 = 18.6%) (Table 4; Fig. 5d) and e)). The first (PC1) shows high positive loadings for 4-ring (0.91), 5-ring (0.86) and 6-ring PAHs (0.59) as well as As (0.78), whereas the second (PC2) is characterized by a strong positive loading for coprostanol (0.83) and an opposing loading for 3-ring PAHs (−0.72) (Table 4).

PAH diagnostic ratios in HZ02 indicate Ant/(Ant+Phe) values consistently>0.1, Fla/(Fla+Pyr) of 0.595-0.951, BaA/(BaA+Chr) of 0.554-0.759, and IcdP/(IcdP+BghiP) of 0.224-0.339. The fecal sterol index FSI = COP/(COP+CHOA) ranged from 0.318 to 0.913 (Fig. 6).

Discussion

Spatial Patterns of PAHs and Sterols Across Haizhou Bay and Centennial Trends Inferred From Core HZ02 (~150 years)

The transport and distribution of contaminants in coastal sediments are strongly shaped by terrestrial

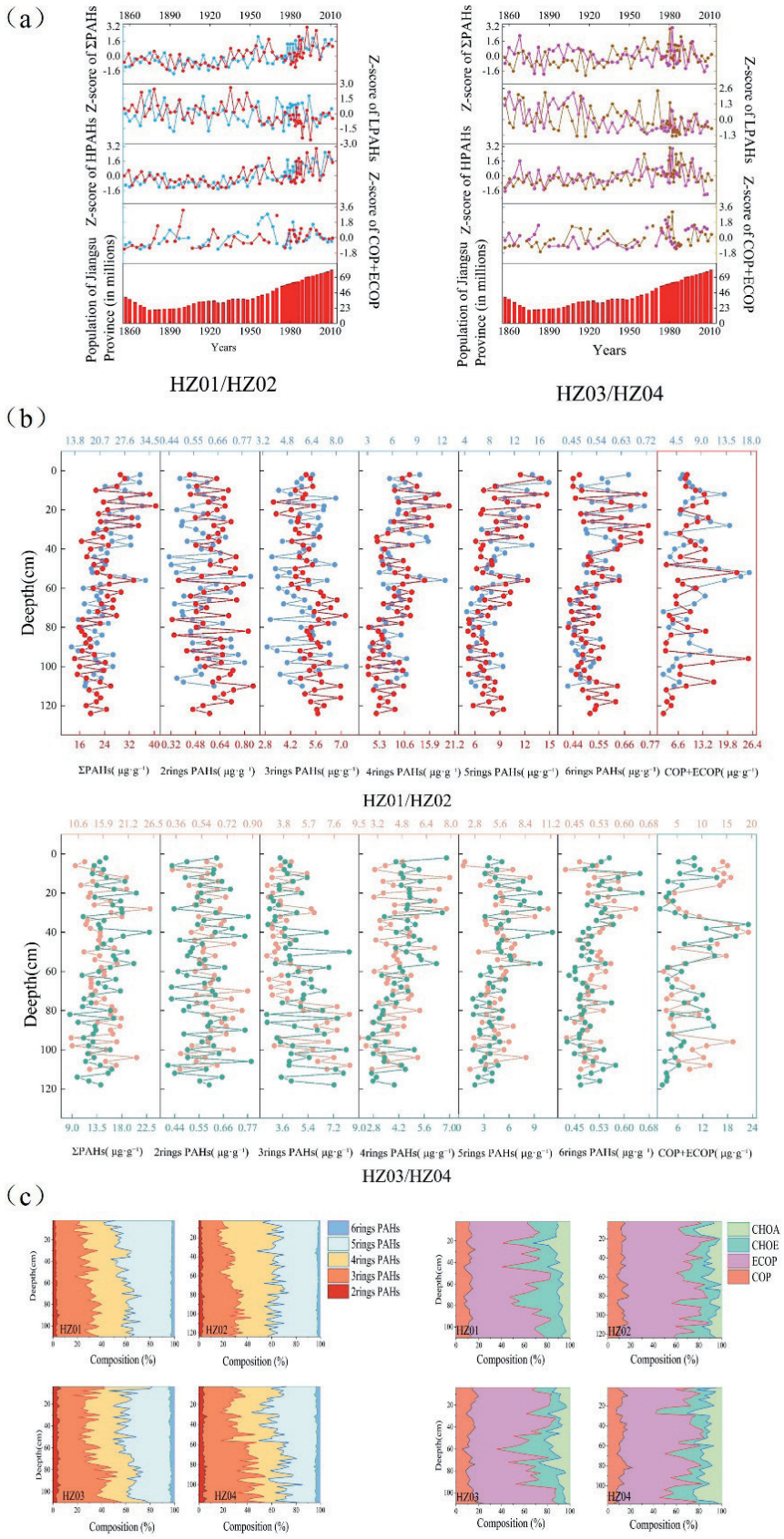

Fig. 4. Spatiotemporal and downcore variations of PAHs and sterols in Haizhou Bay sediment cores. a) Z-score standardized time series of Σ_{16}PAHs, low-ring PAHs (LPAHs; 2-3 rings), high-ring PAHs (HPAHs; 5-6 rings), and COP+ECOP for cores HZ01–HZ04, with colors denoting: HZ01 (blue), HZ02 (red), HZ03 (purple), and HZ04 (brown); Jiangsu population is shown as red bars. b) Depth profiles (μg·g^{-1}) of PAHs and COP+ECOP: the upper panels show HZ01 and HZ02 (HZ01 in blue and HZ02 in red), and the lower panels show HZ03 and HZ04 (HZ03 in orange and HZ04 in green). c) 100% stacked profiles of relative composition (%): the left panels show ring-group PAHs (2-6 rings), and the right panels show sterol composition (COP, ECOP, CHOE, and CHOA).

Table 3. Pearson correlation coefficients (r) among PAH groups, sterol marker(s), and trace metals.

	ΣPAHs	2 Ring PAHs	3 Ring PAHs	4 Ring PAHs	5 Ring PAHs	6 Ring PAHs	As	COP	Ni	Pb	Stanols	Zn
ΣPAHs	1.00	-0.07	-0.04	0.96 ***	0.86 ***	0.46 ***	0.62 ***	0.03	0.17 *	-0.29 ***	0.44 ***	-0.04
2 Ring PAHs	-0.07	1.00	-0.11	-0.02	-0.16 *	0.07	0	0.20 *	-0.01	0.04	-0.09	-0.03
3 Ring PAHs	-0.04	-0.11	1.00	-0.13	-0.19 *	-0.29 ***	-0.50 ***	-0.36 ***	-0.12	0.15	-0.36 ***	0.01
4 Ring PAHs	0.96 ***	-0.02	-0.13	1.00	0.71 ***	0.47 ***	0.68 ***	0.09	0.20 *	-0.32 ***	0.49 ***	-0.01
5 Ring PAHs	0.86 ***	-0.16 *	-0.19 *	0.71 ***	1.00	0.39 ***	0.55 ***	0.04	0.12	-0.21 **	0.38 ***	-0.07
6 Ring PAHs	0.46 ***	0.07	-0.29 ***	0.47 ***	0.39 ***	1.00	0.36 ***	0.21 **	0.07	-0.19 *	0.36 ***	-0.15
As	0.62 ***	0	-0.50 ***	0.68 ***	0.55 ***	0.36 ***	1.00	0.14	0.15	-0.39 ***	0.32 ***	-0.06
COP	0.03	0.20 *	-0.36 ***	0.09	0.04	0.21 **	0.14	1.00	0.23 **	0.36 ***	0.1	0.1
Ni	0.17 *	-0.01	-0.12	0.20 *	0.12	0.07	0.15	0.1	1.00	0.08	0.28 ***	0.86 ***
Pb	-0.29 ***	0.04	0.15	-0.32 ***	-0.21 **	-0.19 *	-0.39 ***	0.23 **	0.08	1.00	-0.49 ***	0.09
stanols	0.44 ***	-0.09	-0.36 ***	0.49 ***	0.38 ***	0.36 ***	0.32 ***	0.36 ***	0.28 ***	-0.49 ***	1.00	0.21 **
Zn	-0.04	-0.03	0.01	-0.01	-0.07	-0.15	-0.06	0.1	0.86 ***	0.09	0.21 **	1.00

Note: * $p<0.05$, ** $p<0.01$, and *** $p<0.001$ (two-tailed).

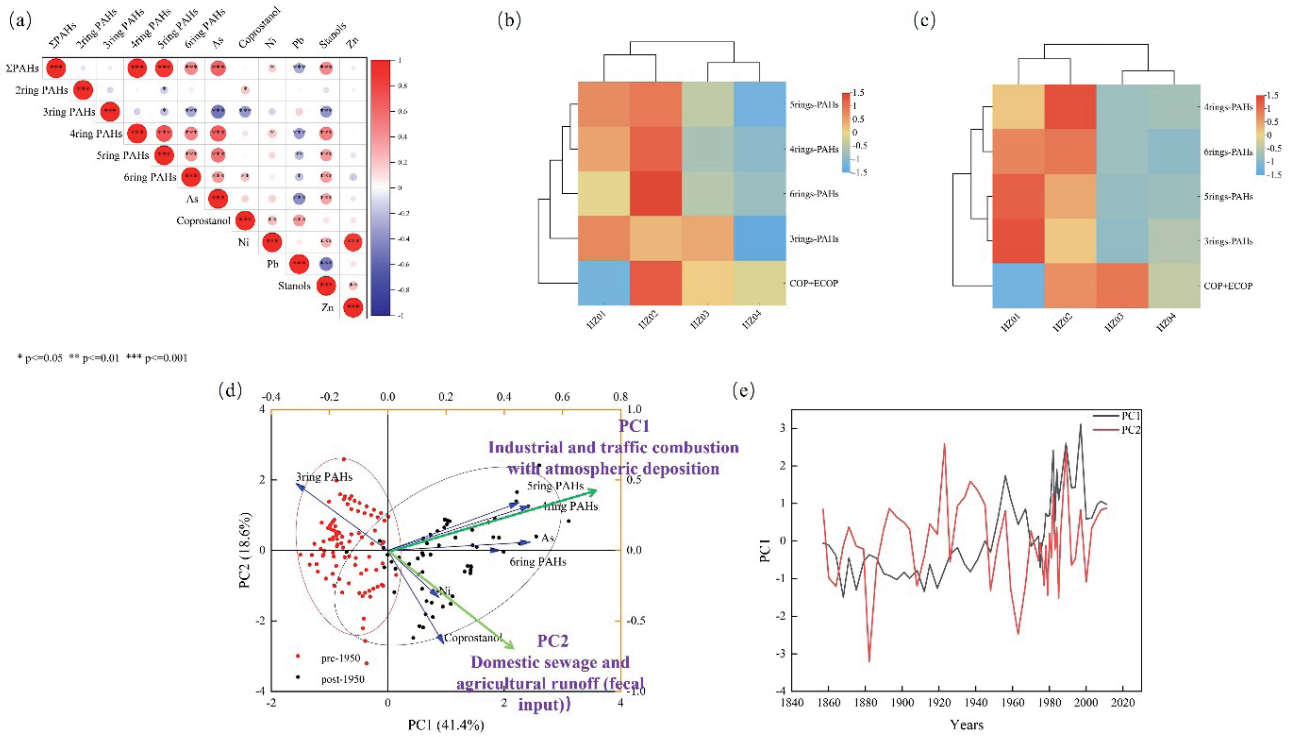

Fig. 5. Multivariate relationships and source-related patterns of PAHs, sterols, and trace metals in Haizhou Bay sediments. a) Pearson correlation matrix among ΣPAHs, ring-grouped PAHs (2-6 rings), coprostanol, total sterols (Stanols), and selected metals (As, Ni, Pb, Zn). Trace-metal concentrations (As, Ni, Pb, and Zn) were compiled from the published dataset for core HZ02 [47] and aligned with the organic records at shared depth intervals. Circle size and color denote correlation strength and direction; significance is indicated as * p<0.05, ** p<0.01, and *** p<0.001; (b-c) Hierarchical cluster analysis (HCA) heatmaps showing standardized (z-score) variations of PAH ring groups and coprostanol + epicoprostanol (COP + ECOP) across cores HZ01–HZ04 for two periods: pre-1950 (b) and post-1950 (c); d) PCA biplot for HZ02, showing sample scores (pre-1950 vs. post-1950) and variable loadings; ellipses indicate group dispersion. PC1 and PC2 explain 41.4% and 18.6% of the variance, respectively. e) Temporal profiles of PCA factor scores (PC1 and PC2) illustrating the evolution of the two dominant components through time.

Table 4. Principal component analysis loadings of the HZ02. Significant values are in bold.

Element	Principal component (PC)	
	PC1	PC2
3-ring PAHs	-0.249	**-0.723**
4-ring PAHs	**0.907**	0.034
5-ring PAHs	**0.860**	-0.016
6-ring PAHs	**0.593**	0.284
As	**0.780**	0.301
Ni	0.104	0.472
Coprostanol	-0.032	**0.825**
Total variance (%)	41.4	18.6
Cumulative (%)	41.4	60
Estimated source	Industrial and traffic combustion with atmospheric deposition	Domestic sewage and agricultural runoff (fecal input)

inputs [50]. Combustion-derived pollutants from biomass and fossil fuels can be transported atmospherically and deposited to nearshore waters as particle-bound aerosols. In parallel, river discharge, groundwater outflow, and surface runoff deliver land-derived contaminants across the land-sea interface to the coastal ocean [3, 51-53]. The spatial contrasts observed among the four cores (Fig. 3 and Fig. 4) therefore reflect the combined effects of source intensity, transport pathways, and depositional sorting.

PAH sources are commonly classified as pyrogenic or petrogenic [54]. Regional geological and historical evidence indicates that the Lianyungang–Haizhou Bay area lies within a weakly active Quaternary tectonic zone and has experienced no volcanic eruptions since the Quaternary, implying negligible contributions from volcanic heat sources [55, 56]. In addition, this coastal sector is not part of China's major offshore hydrocarbon basins, and there are no records of natural oil seepage or major offshore oil-spill accidents in the area [57, 58]. The dominance of medium-to-high ring classes and the substantial contribution of high-molecular-weight PAHs (Fig. 3) are consistent with a predominantly pyrogenic

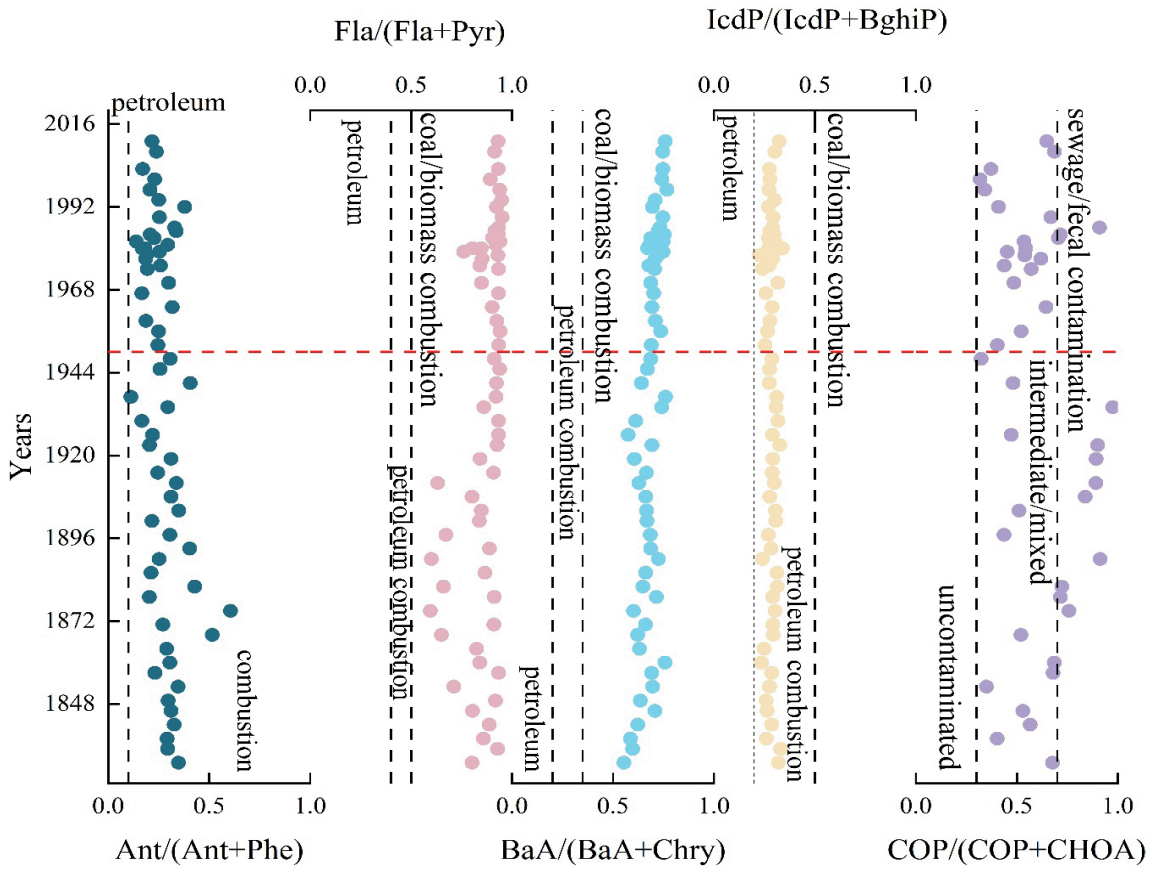

Fig. 6. Down-core temporal variations of PAH diagnostic ratios and the fecal sterol index (FSI) in core HZ02 from Haizhou Bay. PAH source fingerprints include Ant/(Ant+Phe), Fla/(Fla+Pyr), BaA/(BaA+Chry), and IcdP/(IcdP+BghiP), whereas fecal input intensity is evaluated using FSI = COP/(COP+CHOA). Vertical dashed lines denote commonly used threshold ranges for qualitative source interpretation: Ant/(Ant+Phe) < 0.1 (petrogenic) and >0.1 (pyrogenic/combustion); Fla/(Fla+Pyr) <0.4 (petrogenic), 0.4-0.5 (petroleum combustion), and >0.5 (coal/biomass combustion); BaA/(BaA+Chry) <0.2 (petrogenic), 0.2-0.35 (petroleum combustion), and >0.35 (coal/biomass combustion); and IcdP/(IcdP+BghiP) <0.2 (petrogenic), 0.2-0.5 (petroleum combustion), and >0.5 (coal/biomass combustion). For FSI, values <0.3 indicate negligible fecal contamination, 0.3-0.7 indicate intermediate/mixed influence, and >0.7 suggest strong sewage/fecal input. The red dashed horizontal line marks the mid-20th-century transition (≈1950) used to guide stage-wise comparisons.

signature. Previous studies show that combustion-derived PAHs are typically dominated by high-ring compounds, exhibiting a pronounced enrichment of high-molecular-weight PAHs [59, 60]. Taken together, these lines of evidence indicate that PAHs preserved in Haizhou Bay sediments over the past ~150 years are dominated by pyrogenic inputs associated with human activities [45, 61].

The spatial heterogeneity of PAHs in Haizhou Bay is broadly consistent with the distribution of shoreline human activities: Σ_{16}PAHs is higher in the nearshore cores (HZ01 and HZ02) than in the more offshore cores (HZ03 and HZ04) (Fig. 3), indicating a clear seaward decrease. This pattern accords with previous surveys of surface sediments, which attribute PAHs in Haizhou Bay mainly to traffic emissions and coal/biomass combustion [41, 45], and it is consistent with the strong clustering of port infrastructure, nearshore industry, and major transport corridors along the northern coastline of Lianyungang. These observations suggest that nearshore pyrogenic source zones constitute the principal PAH emission areas for the bay.

Beyond local source intensity, monsoon-driven atmospheric transport likely exerts an important control on nearshore enrichment. As a typical embayment along the western Yellow Sea, Haizhou Bay is strongly influenced by the East Asian monsoon; northerly to northwesterly winds prevail in winter [62], placing nearshore waters downwind of terrestrial emissions. Observational and modeling studies in the Yellow Sea and South China Sea indicate that monsoon circulation strongly shapes the spatial distribution of air–sea PAH fluxes: windward sectors commonly experience enhanced dry and wet deposition, which increases coastal input fluxes [23, 63]. Accordingly, the "high nearshore–low offshore" pattern of Σ_{16}PAHs likely reflects the combined influence of coastal pyrogenic emissions and monsoon-modulated atmospheric deposition, rather than being a direct expression of local source strength alone.

In addition, the spatial distribution of PAHs in Haizhou Bay is strongly modulated by their

physicochemical properties and local depositional dynamics. Sediment grain size transitions from fine fractions (e.g., silt) in the northern bay and inner embayment to silty sand and rhythmic interbeds in the outer bay and the southern sector, indicating a seaward increase in hydrodynamic energy [64]. Fine-grained, lower-energy nearshore settings favor particle-associated deposition and promote the enrichment and preservation of hydrophobic HMW PAHs [65, 66], whereas coarser, higher-energy environments offshore are less conducive to retaining particle-bound PAHs. These depositional controls are consistent with the observed cross-bay patterns in PAH concentration and composition (Fig. 3 and Fig. 4).

In contrast, sterols provide a more direct proxy for terrestrial organic-matter inputs, and their spatial distributions are particularly sensitive to the intensity of coastal human activities and watershed delivery pathways. Fecal sterols, produced by microbial reduction of cholesterol in the mammalian gut, are widely used to trace land-derived inputs from domestic sewage, livestock wastes, and agricultural runoff [67-69]. Across the four cores, sterol concentrations were consistently lower in HZ01 and HZ02 than in HZ03 and HZ04. This sterol distribution pattern closely matches the spatial heterogeneity in terrestrial input pathways and alongshore human activities. The Linhong and Shawang rivers are considered major pathways delivering pollutants to Haizhou Bay, and the estuary-adjacent areas act as key depositional sinks for land-derived materials [37]. Moreover, the Linhong estuary and adjacent nearshore waters, which host intensive port operations, industry, and aquaculture, are subject to persistently high anthropogenic inputs of nutrients and organic matter, strengthening the nearshore contamination signal [53]. Accordingly, sterol and fecal sterol concentrations were markedly higher in the cores closer to the Linhong River estuary (HZ03 and HZ04) than in HZ01 and HZ02, indicating stronger terrestrial organic-matter inputs to the estuary-adjacent nearshore zone.

Beyond differences in source strength, sterol distributions in Haizhou Bay are also constrained by molecular properties and depositional conditions. Owing to their strong lipophilicity, sterols readily associate with sedimentary organic matter and tend to accumulate and be preserved in fine-grained, organic-rich settings [70]. Consistent with this pattern, intertidal sediments at HZ03 and HZ04 are dominated by silt–clay fractions, with generally higher fine-particle contents and organic-matter levels than at HZ01 and HZ02 [64], providing favorable conditions for sterol sorption and long-term retention. By contrast, the coarser-grained, higher-energy environments at HZ01 and HZ02 are less conducive to sterol preservation. Thus, the systematic enrichment of sterols at HZ03 and HZ04 likely reflects the combined effects of stronger terrestrial inputs and more favorable depositional conditions.

Overall, the contrasting spatial patterns of PAHs and sterols in Haizhou Bay sediments reflect distinct input pathways and sedimentary controls: PAHs track combustion emissions, atmospheric transport, and particle deposition, whereas sterols are governed mainly by watershed runoff, the spatial distribution of human activities, and organic-matter-rich depositional settings.

To place the contamination levels in Haizhou Bay into a broader regional and global context, we compared the tidal-flat core results with published data from representative estuaries/bays worldwide (Table 5 and Table 6).

For PAHs, the mean Σ_{16}PAHs concentration in the Haizhou Bay tidal-flat core is 19.00±5.805 μg·g^{-1} (Table 5), which is markedly higher than values reported for several relatively low-input systems in China, including the North of Liaodong Bay [71], the Pearl River Delta river network [72], lakes in the middle-lower Yangtze region [73], and the East China Marginal Seas sediments [74], and is also higher than the mean level reported for the Yellow River Delta [75]. At the global scale, Σ16PAHs in Haizhou Bay is lower than the upper levels reported for Toulon Bay

Table 5. Concentration ranges and mean concentrations of Σ_{16}PAHs (μg·g^{-1}) in sediments from Haizhou Bay and other representative estuaries/bays worldwide.

Region	Concentration range (μg·g^{-1})	Mean concentration (μg·g^{-1})	Indicator	Sampling year	Reference
Haizhou Bay tidal flat core	8.614-40.48	19.00±5.805	Σ_{16}PAHs	1857-2014	This study
North of Liaodong Bay	0.192-0.624	0.304	Σ_{16}PAHs	2009	[71]
Pearl River Delta	0.0690-1.297	0.401	Σ_{16}PAHs	2015	[72]
Lakes (middle–lower Yangtze)	0.221-2.419	0.752	Σ_{16}PAHs	1895-2015	[73]
Yellow River delta	3.590-27.11	9.540	Σ_{16}PAHs	2009	[75]
Toulon Bay, France	22.90-182	–	Σ_{16}PAHs	–	[76]
Narragansett Bay, USA	0.569-216	21.100	Σ_{44}PAHs		[77]
Gulf of Kutch, India	18.28-1099	321.6	Σ_{16}PAHs	–	[78]
ECMSs sediments, China	0.004-1.636	0.660±0.330	Σ_{16}PAHs	2014-2016	[74]

Table 6. Concentration ranges and mean concentrations of sterol indicators (μg·g^{-1}) in sediments from Haizhou Bay and other study regions worldwide (definitions follow this study).

Region	Concentration range (μg·g^{-1})	Mean concentration (μg·g^{-1})	Indicator	Sampling year	Reference
Haizhou Bay tidal flat core	2.971-31.89	11.66	COP+ECOP+CHOE+CHOA	1857-2014	This study
Danube sediment, Serbia	0.022-1.939	-	COP+ECOP+CHOE+CHOA		[79]
The north coast of New South Wales, Australia.	-	2036.026	COP+ECOP		[82]
Brazilian mangroves	2.500-39.03		Total fecal sterols		[80]
Siak River, Indonesia	0.050-10.530	0.878	COP		[81]

(France) [76] and Narragansett Bay (USA) [77], and is far below the heavily contaminated Gulf of Kutch (India) [78], indicating an overall moderate level of PAH contamination.

For sterols, Σ_4 sterols (COP+ECOP+CHOE+CHOA) in the Haizhou Bay tidal-flat core ranges from 2.971 to 31.89 μg·g^{-1} with a mean of 11.66 μg·g^{-1} (Table 6). This level exceeds that reported for Danube sediments [70], is comparable in magnitude to the reported range of total fecal sterols in Brazilian mangroves [79], and is higher than the mean coprostanol level in the Siak River (Indonesia) [80], but remains far below the extremely high value reported for the North coast of New South Wales (Australia) [81]. These contrasts indicate that sterol indicators can vary widely among regions, reflecting combined controls of sewage loading intensity, catchment delivery efficiency, and depositional conditions on sterol accumulation and preservation.

Overall, the regional–global comparison provides a reference framework for assessing the level of mixed contamination in Haizhou Bay and establishes a contextual baseline for subsequent discussion of downcore variations in pollutant concentrations and composition in the age-constrained sediment-core record, as well as their potential driving factors. Building on this regional-global context, we next examine the dated HZ02 core to interpret centennial-scale changes in contaminant concentrations and composition (Fig. 4).

The dated HZ02 sediment-core record spanning the past ~150 years shows sustained accumulation of Σ_{16}PAHs and fecal sterols in Haizhou Bay since the mid-to-late nineteenth century. Their composition shifted from early dominance of low-ring PAHs to a high-ring-dominated assemblage from the mid-to-late twentieth century onwards, broadly tracking the regional trajectory of industrialization (Fig. 4).

In the dated HZ02 record during 1850-1950, low-ring PAHs increased episodically, with 3-ring compounds dominating the assemblage. Because 3-ring PAHs are commonly used as indicators of biomass combustion, their enrichment points to substantial contributions from the burning of wood, crop residues, and other traditional biofuels [7, 82]. Sterol concentrations in HZ02 also increased during this period; notably, fecal sterols track domestic sewage inputs [16], suggesting strengthened household-derived loading. The co-variation of PAHs and sterols therefore indicates that, under population recovery, pollution levels were jointly driven by a biomass-based energy structure and increasing sewage discharge. From 1950 to 1980 in core HZ02, concentrations of all PAH groups and sterols rose sharply, and high-ring PAHs became dominant, indicating a substantive shift in source structure. Intensified coal combustion is known to increase the relative contribution of high-ring PAHs to emissions [83]. Meanwhile, under rapid urbanization, lagging development of wastewater-treatment infrastructure can sustain growth in sewage discharge, promoting the accumulation of fecal sterols in sediments [84]. Sedimentary evidence further suggests that since the mid-twentieth century, industrialization, energy consumption, and urban expansion in the Haizhou Bay region accelerated in parallel with rising pollutant loads [85]. Consistent with this regional trajectory, the marked increases in PAHs and sterols observed here coincide with a rapid transition from biomass to coal and with concurrent population growth.

During 1980-2000 in core HZ02, 5-6-ring PAHs and fecal sterols reached their maxima, indicating pronounced intensification of contaminant loading. Following China's Reform and Opening-up, rapid expansion of coastal ports in eastern China, together with rising transport-fuel consumption and industrial combustion emissions, substantially increased the relative contribution of high-ring PAHs [86]. Over the same period, population growth and accelerated coastal urban expansion sustained increases in domestic wastewater discharge, further promoting fecal-sterol accumulation. The sediment record thus captures a clear regional response to the combined effects of changing fuel-use structure and urbanization. Since the early twenty-first century in HZ02, concentrations of high-ring PAHs and sterols have declined markedly, coincident with sustained implementation of national pollution-control policies, suggesting persistent region-scale benefits of emission mitigation. Comparable downturns have been documented in sediment records from other major estuary-bay systems in China, including the Yangtze and Pearl River estuaries [87, 88].

Overall, PAH concentrations were substantially higher in the nearshore cores (HZ01 and HZ02) than in the more offshore cores (HZ03 and HZ04), decreasing seaward with increasing distance from the coastline. In contrast, sterols were enriched in cores proximal to the Linhong River estuary, consistent with strengthened terrestrial organic-matter inputs from domestic sewage and agricultural runoff. Temporally, the dated HZ02 record indicates that 1860-1950 was characterized by dominance of low-ring PAHs and comparatively low levels of high-ring PAHs and sterols; from 1950 to 2000, high-ring PAHs and fecal sterols increased in concert; and since the early twenty-first century both have declined overall, although the domestic-source signal remains pronounced near the Linhong River estuary. Collectively, the HZ02 sediment record indicates nearshore enrichment of PAHs and estuary-focused accumulation of sterols, together with a long-term shift from early low-ring PAH dominance to mid-late twentieth-century increases in high-ring PAHs and fecal sterols, followed by a recent decline. These trends reflect progressive reorganization of pollution sources through industrialization and subsequent pollution-control efforts.

Source Apportionment of Mixed PAH-Sterol-Heavy Metal Contamination in Haizhou Bay Over the Past ~150 Years

We conducted an integrated assessment of the relationships among PAHs, sterols, and heavy metals across the four Haizhou Bay sediment cores, and interpreted centennial-scale (~150-year) temporal coupling primarily based on the dated HZ02 record (Fig. 5).

Correlation analysis (Fig. 5a)) shows a significant positive relationship between PAHs and sterols (COP, ECOP, CHOA, and CHOE). In the York River estuary (Virginia, USA), sterols were also positively correlated with Σ_{16}PAHs, and analyses of particulate organic matter and lipid biomarkers indicated that both compound classes were associated with terrestrial organic matter and anthropogenic inputs [89]. Together, these lines of evidence suggest that PAHs and sterols in Haizhou Bay may share partially overlapping terrestrial sources and input pathways. High-ring PAHs (4-6 rings) further exhibit significant positive correlations with As and sterols (Fig. 5a)), consistent with observations from eastern China's coast and the Yangtze River estuary where co-enrichment of high-ring PAHs with As/Ni has been linked to fossil-fuel combustion emissions [82, 90]. In addition, fecal sterols show significant associations with selected trace metals (Fig. 5a)), consistent with evidence that domestic wastewater and agricultural runoff can contribute jointly to the coupling between fecal biomarkers and trace metals in large river-lake systems [91]. Overall, these relationships indicate that both domestic inputs and combustion/industrial emissions contribute to the co-distribution of organic and inorganic contaminants in Haizhou Bay sediments.

Hierarchical clustering of the dated HZ02 record (Fig. 5b) and c)) indicates that contaminants formed two major groups during the 1850-1950 interval (Fig. 5b)). Group I comprised mainly 3-ring PAHs together with fecal sterols (COP + ECOP), whereas Group II was dominated by 4-6-ring PAHs. Previous studies suggest that 3-ring PAHs are closely associated with wood and crop-residue burning [4], although agricultural burning and wildfires can also generate a measurable fraction of high-ring PAHs under high-temperature conditions [7]. By contrast, 4-ring PAHs are often linked to low-to-moderate temperature coal combustion, whereas 5-6-ring PAHs predominantly derive from high-temperature combustion of coal and other fossil fuels. Once emitted, these compounds are commonly transported in the gas and particle phases and subsequently deposited and preserved in sediments [92]. Fecal sterols are established indicators of human and livestock waste contamination, derived primarily from domestic sewage discharge and agricultural runoff [16, 68]. Accordingly, the cluster linking 3-ring PAHs with COP + ECOP likely reflects the combined influence of biomass burning and domestic–livestock inputs, whereas the cluster dominated by 4-6-ring PAHs is more consistent with atmospherically transported combustion-derived inputs. Taken together, the 1850-1950 grouping suggests a relatively low-intensity, land-based contamination regime dominated by biomass fuel use and domestic/agricultural inputs. After 1950 in the HZ02 chronology (Fig. 5c)), the clustering structure reorganized markedly. All PAH homologues (3-6 rings) grouped together, indicating coherent co-variation among ring classes across sites and suggesting control by broadly shared combustion emissions and atmospheric deposition at the catchment-nearshore-bay scale. Given that high-ring PAHs are closely associated with high-temperature combustion, this pattern is consistent with integrated inputs from fossil-fuel-related sources, including coal burning, traffic emissions, and industrial combustion. In contrast, COP + ECOP formed a distinct branch separated from the PAH cluster, implying that sterols were governed by transport pathways different from those of combustion-derived PAHs. Because sterols primarily originate from domestic wastewater and terrestrial runoff, their spatial pattern is more likely dominated by estuary–nearshore delivery intensity. This shift in cluster structure parallels the documented transition from biomass burning to fossil-fuel combustion in China's coastal sediments [61], suggesting a comparable post-1950 shift in energy use and combustion emissions in Haizhou Bay. Across the full dataset, samples from HZ01-HZ02 and HZ03-HZ04 tend to cluster separately, indicating persistent contrasts in contaminant composition between nearshore and offshore settings. These differences likely reflect gradients in distance from shore, the strength of terrestrial inputs, and hydrodynamic sorting, highlighting that contaminant

distributions in Haizhou Bay are jointly shaped by multiple spatial processes.

PAH diagnostic ratios were applied as supporting fingerprints to further constrain combustion sources in the dated representative core HZ02 (Fig. 6). Source assignments followed the commonly adopted threshold framework for Ant/(Ant+Phe), Fla/(Fla+Pyr), BaA/(BaA+Chr), and IcdP/(IcdP+BghiP), which has been widely applied to distinguish petrogenic versus pyrogenic inputs and combustion subtypes in aquatic sediments [7]. In this study, Ant/(Ant+Phe) values consistently exceeded 0.1, indicating predominantly pyrogenic inputs rather than direct petrogenic contamination. Fla/(Fla+Pyr) and BaA/(BaA+Chr) further support this interpretation, as both ratios largely fall within the coal/biomass-combustion domain. Similar coal/biomass-combustion signatures have been reported in coastal sediments from the Yellow Sea and adjacent Chinese marginal seas, reflecting the long-term dominance of coal use and biomass burning in the region [61, 93]. Meanwhile, IcdP/(IcdP+BghiP) values mainly lie within the 0.2-0.5 interval that is typically associated with petroleum-combustion influences. This suggests that liquid fossil-fuel combustion (e.g., traffic-related emissions) has been persistently superimposed on the dominant coal/biomass signal, although this ratio may also capture mixed combustion sources in complex coastal settings. Taken together, these ratios indicate mixed combustion sources dominated by coal/biomass burning with additional petroleum-combustion contributions, consistent with the co-variation patterns and source factors identified by hierarchical clustering and PCA (Fig. 5). To evaluate fecal inputs, a fecal sterol index was calculated for core HZ02 as FSI = COP/(COP+CHOA) (Fig. 6). Following commonly used classifications, FSI values <0.3 indicate negligible fecal contamination, whereas values >0.7 suggest strong sewage/fecal influence [16, 68]. The observed FSI range indicates intermediate-to-strong fecal influence across the record, in agreement with the enrichment of fecal sterols observed in the correlation and clustering analyses (Fig. 5a) and c)). It should be noted that diagnostic ratios and sterol indices may be influenced by source mixing and post-depositional processes; therefore, they are best interpreted as qualitative supporting lines of evidence rather than standalone quantitative apportionment tools [94].

Principal component analysis (PCA) was used to identify the dominant factors governing coupled PAH–sterol contamination in Haizhou Bay sediments. PC1 and PC2 (Table 4; Fig. 5d) and e)) explained ~60% of the total variance (PC1 = 41.4%, PC2 = 18.6%; cumulative = 59.9%). The dataset met the requirements for factor analysis, as indicated by the Kaiser–Meyer–Olkin (KMO) measure (0.64) and a significant Bartlett's test of sphericity [95, 96]. Temporal changes in factor scores further reveal stage-wise shifts in source influence (Fig. 5e)). PC1 accounted for 41.4% of the variance and was characterized by high positive loadings for 4-6-ring PAHs and As (0.91, 0.86, 0.59, and 0.78, respectively). High-molecular-weight PAHs (4-6 rings) are typically associated with high-temperature incomplete combustion of fossil fuels and related organic matter [97, 98]. Arsenic is also widely used as a diagnostic tracer of coal combustion and industrial emissions [99]. Sediment records from the Bohai and Yellow seas indicate that regional PAH burdens largely reflect industrial activity, traffic emissions, and coal burning; high-ring PAHs are emitted to the atmosphere in both gas and particle phases and are delivered to adjacent coastal waters through short-range transport followed by dry and wet deposition [93]. Consistent with this interpretation, core HZ02 shows markedly increased accumulation of high-temperature combustion-derived PAHs in recent decades, with high-ring compounds becoming compositionally dominant, and previous source apportionment attributes bay PAHs to biomass burning, traffic emissions, and atmospherically transported combustion inputs [85]. Collectively, PC1 most likely represents a mixed input driven by high-temperature industrial combustion and subsequent atmospheric deposition. PC2 explained 18.6% of the total variance and was characterized by a strong positive loading for coprostanol (0.83) coupled with an opposing, significant loading for 3-ring PAHs (−0.72). Coprostanol is a well-established molecular tracer of human and livestock fecal inputs; its enrichment in sediments generally reflects sustained delivery of terrestrial organic matter to bay systems via domestic sewage and agriculturally influenced runoff [100]. Previous work further indicates that intensifying agriculture and urbanization in the Haizhou Bay region – through expanded irrigation, livestock production, and increased sewage discharge – has strengthened fecal-source loading [101]. Accordingly, PC2 is most parsimoniously interpreted as a fecal-input gradient dominated by domestic wastewater and agricultural runoff, while the opposing loading of 3-ring PAHs indicates statistical separation between fecal-source influence and low-ring PAH background within the dataset. In the dated HZ02 record, the early interval (1850-1950) was dominated by 3-ring PAHs, whereas in the modern period (1950-2011) the contributions of 4-6-ring PAHs and As increased markedly, indicating a progressive shift in the regional energy structure from biomass combustion toward coal use, motor-vehicle emissions, and high-temperature industrial combustion. This trajectory is consistent with the ~200-year sediment record from Liaodong Bay, where natural fires and wood burning prevailed prior to industrialization, followed by coal combustion and vehicle fuels becoming dominant sources [61]. The HZ02 factor-score series further supports this transition: before 1950, PC1 scores remained low while PC2 scores were relatively high, consistent with pollution dominated by biomass burning and domestic inputs. From ~1950 onward, PC1 increased steadily and peaked during 1980-2000 (Fig. 5e)), coinciding

with rapid regional industrialization and growth in energy consumption and aligning with the onset of the Anthropocene signal and intensified industrial activity inferred from the Sihailongwan sediment archive [102]. Since the early twenty-first century, both PC1 and PC2 scores have declined, suggesting that although high-temperature combustion remains influential, pollution-control measures and gradual optimization of the energy mix have begun to exert measurable effects [103]. Overall, the HZ02 PCA results capture a temporal shift from biomass burning and domestic inputs to fossil-fuel and industrial and traffic influences, followed by an early twenty-first-century moderation consistent with strengthened emission control and management interventions.

Multiple statistical approaches converge on the same inference: mixed contamination in Haizhou Bay sediments is jointly governed by (i) domestic-agricultural inputs and (ii) high-temperature combustion sources associated with traffic and industry. The dated HZ02 archive indicates that before the mid-twentieth century, contamination was dominated by biomass burning and domestic sewage inputs, before shifting toward a fossil-fuel regime characterized by traffic emissions and coal- and industrial-combustion signatures, with maxima reached in the late twentieth century. This trajectory provides a systematic record of how industrialization and urbanization restructured terrestrial pollution inputs and imposed long-term impacts on the nearshore depositional environment.

History of Contaminant Burial in Haizhou Bay Inferred from the Dated Core HZ02 (~150 Years) and Its Response to Shifts in Energy Structure and Human Activities

The dated HZ02 sediment record shows that, over the past ~150 years, the phased evolution of PAHs, sterols, and trace metals closely tracks regional energy-transition pathways, intensified industrial activity and shifts in population patterns. Collectively, this archive (supported by spatial patterns across the four cores) highlights the long-term control of anthropogenic processes – combustion emissions, atmospheric deposition, and urban wastewater inputs – on the depositional environment.

In the dated HZ02 record during the pre-industrial period (1850-1950), low-ring PAHs and fecal sterols showed pronounced variability. Low-ring PAHs accounted for 25.8-46.2% of total PAHs, while fecal sterols comprised 56.2-89.1% of total sterols (Fig. 7a) and d)). PCA results (Fig. 5d) and e)) indicate that 3-ring PAHs together with COP + ECOP dominated the contaminant distribution during this interval in HZ02. In the Lianyungang region (then administratively including Ganyu, Guanyun, and Donghai counties), the economy was largely agriculture-based and an industrial system had yet to develop. Local gazetteers and historical–geographical studies suggest that from the late nineteenth century to the mid-twentieth century, rice, wheat, and cotton cultivation dominated production in the northern Jiangsu coastal counties, and rural energy supply relied primarily on traditional biomass fuels such as firewood and crop residues [104]. This agriculture-dominated economy, with limited industrial combustion, provides a plausible context for the predominance of low-ring PAHs, consistent with a biomass-combustion signal indicated by 3-ring PAHs [61, 105]. Fecal sterols, as diagnostic markers of human and animal excreta [16, 68], remained proportionally high during this interval, consistent with widespread livestock husbandry. Historical records report a provincial livestock stock of ~30 million animals in Jiangsu, dominated by poultry [106]; temporal changes in livestock abundance and distribution may therefore have strengthened fecal-sterol inputs. Overall, the co-variation of PAHs and fecal sterols during 1850-1950 reflects an early anthropogenic regime shaped mainly by biomass fuel use and livestock-related inputs, leaving a persistent imprint on the depositional environment.

During 1950-1980 in the HZ02 chronology, sedimentary PAH concentrations increased markedly, accompanied by a compositional shift from low-ring compounds toward 5–6-ring PAHs. High-ring PAHs accounted for 29.1-52.4% of total PAHs in this interval. In parallel, industrial output rose, rural labor increasingly concentrated in urban centers, population density increased, and cultivated land declined (Fig. 7a) and d)). PCA indicates a close association between high-molecular-weight PAHs and As, with PC1 explaining 41.4% of the variance, consistent with strengthened inputs from high-temperature combustion sources. This interval broadly overlaps with China's First to Third Five-Year Plans (1953–1978), when national development priorities strongly favored heavy industry. Against this policy backdrop, Lianyungang and the surrounding areas experienced pronounced land-use conversion and restructuring of energy consumption. For example, construction land in Jiangsu Province expanded from 103.66 km² to 996.25 km² [107]. Statistical records indicate that Lianyungang's industrial GDP increased from 0.48 to 4.23×10^8 CNY (about eightfold), total energy consumption rose from 51.04 to 602.8 Mtce (about twelvefold), population density increased from 247.4 to 509.5 persons km^{-2} (about twofold), and the urbanization rate rose from 10% to 11.8% [43]. These concurrent socioeconomic shifts and changes in energy use are consistent with a substantial rise in emissions of high-ring PAHs and As during this period.

During the period of rapid economic growth (1980-2000), PAHs, sterols, and As increased synchronously and reached their maxima in Haizhou Bay sediments (Fig. 7a) and d)). The marked strengthening of high-ring PAHs indicates sustained intensification of high-temperature combustion inputs. In PCA space, samples from this interval tend to plot with positive scores on both PC1 and PC2, consistent with joint influences from

combustion-related emissions and strengthened urban-catchment delivery. Previous studies report sustained increases in multiple heavy metals in Haizhou Bay sediments since the 1980s, closely tracking the clustering of industrial enterprises and regional industrialization in Lianyungang [47]. Over the same period, continued discharge from the Linhong and Shawang rivers strengthened catchment-derived inputs of metals and industrial organic contaminants to the bay [108]. Since the 1990s, nearshore sediments along the northern Jiangsu coast have shown enrichment of 5-6-ring PAHs, attributed mainly to industrial fossil-fuel combustion and traffic emissions [41, 45]. This pattern aligns with rapid growth in port throughput, rising transport-fuel consumption, and accelerating urbanization, together with sustained wastewater and industrial contaminant delivery to estuarine and nearshore zones [109, 110]. Overall, the late-twentieth-century record captures a characteristic mixed-contamination regime shaped by the combined effects of industrial combustion, atmospheric deposition, and catchment inputs.

Since the early twenty-first century in HZ02, port throughput, population density, and industrial-agricultural output in Lianyungang have continued to rise, yet concentrations of PAHs, sterols, and As in Haizhou Bay sediments have declined systematically (Fig. 7). This divergence indicates that the relationship between economic expansion and contaminant loading has weakened, consistent with concurrent changes in China's energy system and improvements in wastewater management. National power-sector statistics indicate that, between 2000 and 2020, the share of coal-fired generation decreased while non-fossil electricity expanded, lowering the emission intensity of electricity production by ~20–30% [111, 112]. In parallel, municipal wastewater-treatment capacity expanded rapidly, and the centralized urban sewage-treatment rate increased from <20% in the late twentieth century to >90% by the late 2010s [113, 114]. Local statistics further suggest that Lianyungang underwent structural adjustments during 2000-2010 that mirrored national trends. Agriculture's share of the total output value of farming, forestry, animal husbandry, and fisheries declined from 59.8% to 47.4%, implying a relative weakening of traditional agricultural activities and associated biomass-fuel use. Meanwhile, regional electricity generation increased from 7.15 to 51.88 million kWh, whereas raw-coal output decreased, pointing to a gradual shift toward

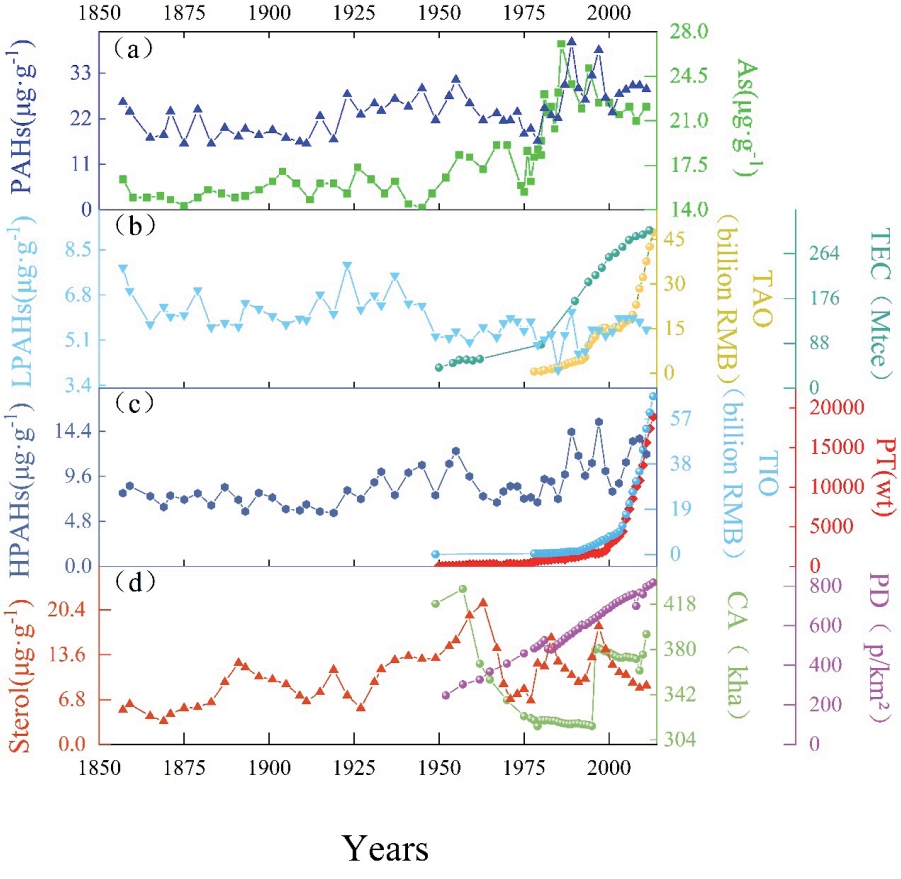

Fig. 7. Time-series comparison between sedimentary contaminant proxies and regional socioeconomic indicators in Haizhou Bay. a) Downcore profiles of Σ_{16}PAHs and As; b) low-molecular-weight PAHs (LPAHs) plotted alongside total agricultural output (TAO) and total energy consumption (TEC); c) high-molecular-weight PAHs (HPAHs) plotted alongside total industrial output (TIO) and port throughput (PT); and d) total sterols plotted alongside cultivated land area (CA) and population density (PD). Contaminant concentrations are reported in μg g^{-1}, whereas socioeconomic indicators are shown on the right y-axes.

a more centralized and efficient energy-supply system [43]. Together, these shifts imply reduced combustion-related emissions and lower direct land-based loads per unit of economic activity. Sterol-based evidence further suggests that improved wastewater-treatment performance can substantially reduce fecal-sterol discharge to nearby coastal waters [115]. Accordingly, the coherent declines of multiple contaminants in Haizhou Bay sediments most likely reflect the combined effects of cleaner energy use, tighter emission controls, and upgraded wastewater management.

Overall, the dated HZ02 archive traces a clear ~150-year trajectory of pollutant inputs that parallels major shifts in energy use and human activities. An early agrarian stage was dominated by biomass burning and domestic emissions, with PAHs characterized mainly by low-ring compounds. With mid-twentieth-century industrialization, the energy base shifted toward coal, and high-ring PAHs increased sharply, producing a distinct industrial-combustion imprint. During 1980-2000, industrial expansion, rising transport demand, and port development jointly amplified the accumulation of multiple contaminant classes. Since the early twenty-first century, contaminant levels have declined overall, consistent with energy-system optimization and strengthened pollution control. Together, this sequence highlights the long-term influence of energy transitions, industrialization, and mitigation efforts on the regional contaminant regime.

Conclusions

Coastal sediments provide one of the most enduring archives of Anthropocene pollution. Using an ~150-year sediment sequence constrained by the published $^{210}Pb_{ex}$–^{137}Cs chronology of core HZ02 from Haizhou Bay, we applied an integrated, multi-proxy framework to quantify the spatiotemporal patterns, source structure, and socioeconomic linkages of PAHs, sterols, and heavy metals. PAH concentrations decreased seaward, whereas sterols were strongly enriched near the Linhong River estuary. The dated HZ02 profile indicates that low-ring PAHs dominated before 1950, followed by episodic increases in high-ring PAHs and sterols during the 1950s-1960s and again in the 1980s-1990s. Sterol concentrations declined in the early twenty-first century, consistent with adjustments in domestic-waste inputs. Overall, the results identify energy-system optimization, industrial policy shifts, and strengthened pollution control as key drivers of improved coastal environmental quality. This study provides a scientific basis for assessing mixed contamination and Anthropocene environmental change in rapidly urbanizing coastal regions, and underscores the importance of regulation and ecosystem-based management for pollution prevention and water-quality protection. Future work should integrate water-sediment-biota processes to resolve transport pathways and ecological effects, thereby supporting region-specific diagnosis and multi-scale mitigation strategies.

Acknowledgments

This research was supported by the National Natural Science Foundation of China (No. 42373085) and the State Key Laboratory of Loess and Quaternary Geology, Chinese Academy of Sciences (No. SKLLQG 2223). We gratefully acknowledge the helpful and valuable comments by the editor and the anonymous reviewers. Finally, we sincerely thank all those for their efforts and contributions to the accomplishment of this research. Many thanks!

Author Contributions

Dong Mu: Writing – original draft, Writing – review and editing, Software, Formal analysis. Zhihai Tan: Conceptualization, Methodology, Investigation, Supervision, Project administration, Resources, Funding acquisition, Writing – review and editing. Longjiang Mao: Investigation, Resources, Funding acquisition. Hao Lei: Formal analysis, Software, Data curation. Chenhao Xi: Investigation, Visualization. Jihong Miao: Investigation, Validation. Juan Li: Investigation, Validation.

AI Usage Disclosure Statement

During the preparation of this manuscript, the authors used ChatGPT for language polishing, grammar checking, and improving the clarity of English expression. The AI tool was not used for data generation, experimental design, statistical analysis, figure preparation, interpretation of results, or drawing scientific conclusions. All AI-assisted text was carefully reviewed, revised, validated, and approved by the authors. The authors take full responsibility for the accuracy, integrity, and originality of the manuscript.

Conflict of Interest

The authors declare no conflict of interest.

References

1. WATERS C.N., ZALASIEWICZ J., SUMMERHAYES C., BARNOSKY A.D., POIRIER C., GAŁUSZKA A., CEARRETA A., EDGEWORTH M., ELLIS E.C., ELLIS M., JEANDEL C., LEINFELDER R., MCNEILL J.R., RICHTER D.D., STEFFEN W., SYVITSKI J., VIDAS D., WAGREICH M., WILLIAMS M., ZHISHENG A., GRINEVALD J., ODADA E., ORESKES N., WOLFE A.P. The Anthropocene is functionally and stratigraphically

distinct from the Holocene. Science, **351** (6269), aad2622, **2016**.
2. WATERS C.N., TURNER S.D. Defining the onset of the Anthropocene. Science, **378** (6621), 706, **2022**.
3. SYVITSKI J.P.M., KETTNER A.J., OVEREEM I., HUTTON E.W.H., HANNON M.T., BRAKENRIDGE G.R., DAY J., VÖRÖSMARTY C., SAITO Y., GIOSAN L., NICHOLLS R.J. Sinking deltas due to human activities. Nature Geoscience, **2** (10), 681, **2009**.
4. BI C., WANG X., JIA J., CHEN Z. Spatial variation and sources of polycyclic aromatic hydrocarbons influenced by intensive land use in an urbanized river network of East China. Science of The Total Environment, **627**, 671, **2018**.
5. BARLETTA M., LIMA A.R.A., COSTA M.F. Distribution, sources and consequences of nutrients, persistent organic pollutants, metals and microplastics in South American estuaries. Science of The Total Environment, **651** (Pt 1), 1199, **2019**.
6. CHEN C.-F., CHEN C.-W., JU Y.-R., DONG C.-D. Vertical profile, source apportionment, and toxicity of PAHs in sediment cores of a wharf near the coal-based steel refining industrial zone in Kaohsiung, Taiwan. Environmental Science and Pollution Research, **23** (5), 4786, **2016**.
7. YUNKER M.B., MACDONALD R.W., VINGARZAN R., MITCHELL R.H., GOYETTE D., SYLVESTRE S. PAHs in the Fraser River basin: a critical appraisal of PAH ratios as indicators of PAH source and composition. Organic Geochemistry, **33** (4), 489, **2002**.
8. ACHARYA S., STROBEL P., PROCHNOW M., TAUT S., ZECH M., SCHWALB A., ZECH R. Paleoclimate, paleoenvironment, and human impact over the last 400 years based on lipid biomarkers from Lake Höglwörth, Germany. Quaternary Science Advances, **15**, **2024**.
9. ABEDI E., NOZARPOUR R. Assessment of PAH and heavy metal contamination in the pars special economic energy zone surface sediments: ecological implications and source identification. Environmental Science and Pollution Research, **32** (41), 23574, **2025**.
10. MOSTERT M.M.R., AYOKO G.A., KOKOT S. Application of chemometrics to analysis of soil pollutants. TrAC Trends in Analytical Chemistry, **29** (5), 430, **2010**.
11. DURAN R., CRAVO-LAUREAU C. Role of environmental factors and microorganisms in determining the fate of polycyclic aromatic hydrocarbons in the marine environment. FEMS Microbiology Reviews, **40** (6), 814, **2016**.
12. ZHAO W., LI J., LU J., LAN T., ZANG L., GUO J., LI T. Polycyclic Aromatic Hydrocarbons (PAHs) in Main urban area Soils of Changchun, Northeast China: Status, Sources, and Potential Toxic Risk Assessment. Polish Journal of Environmental Studies, **31** (3), 2943, **2022**.
13. D'ANJOU R.M., BRADLEY R.S., BALASCIO N.L., FINKELSTEIN D.B. Climate impacts on human settlement and agricultural activities in northern Norway revealed through sediment biogeochemistry. Proceedings of the National Academy of Sciences of the United States of America. **109** (50), 20332, **2012**.
14. LLOYD C.E.M., MICHAELIDES K., CHADWICK D.R., DUNGAIT J.A.J., EVERSHED R.P. Tracing the flow-driven vertical transport of livestock-derived organic matter through soil using biomarkers. Organic Geochemistry, **43** (1), 56, **2011**.
15. DUDA M.P., HARGAN K.E., MICHELUTTI N., BLAIS J.M., GROOMS C., GILCHRIST H.G., MALLORY M.L., ROBERTSON G.J., SMOL J.P. Reconstructing Long-Term Changes in Avian Populations Using Lake Sediments: Opening a Window Onto the Past. Frontiers in Ecology and Evolution, **9**, **2021**.
16. LEEMING R., BALL A., ASHBOLT N., NICHOLS P. Using faecal sterols from humans and animals to distinguish faecal pollution in receiving waters. Water Research, **30** (12), 2893, **1996**.
17. CUNLIN L., LIPING Z., JIANTING J., QINGFENG M., JUNBO W., QIANGQIANG K. Impacts of human and herbivorous feces on lake surface sediments of the Tibetan Plateau based on fecal stanol proxies. Ecological Indicators, **158**, 111487, **2024**.
18. LI R., YUAN Y., LI C., SUN W., YANG M., WANG X. Environmental Health and Ecological Risk Assessment of Soil Heavy Metal Pollution in the Coastal Cities of Estuarine Bay – A Case Study of Hangzhou Bay, China. Toxics, **8** (3), **2020**.
19. GENG N., XIA Y., LI D., BAI F., XU C. Migration and Transformation of Heavy Metal and Its Fate in Intertidal Sediments: A Review. Processes, **12** (2), **2024**.
20. FENG J., YU H., WANG Y., LIU X., YANG M., WANG J., DU P., LI Z. Pollution Assessment and Source Apportionment of Heavy Metals in Sediments of Subsidence Section of Luling Mine in the Tuohe River, China. Polish Journal of Environmental Studies, **34** (2), 1529, **2025**.
21. CAI Y., WANG X., WU Y., LI Y., YA M. Over 100-year sedimentary record of polycyclic aromatic hydrocarbons (PAHs) and organochlorine compounds (OCs) in the continental shelf of the East China Sea. Environmental Pollution, **219**, 774, **2016**.
22. MAN X., SUN J., XIANG Y., SU H., HUANG H., GU Y., ZHANG H., JORDAN R. W., JIANG S. Centennial-scale evolution, source apportionment, and ecological risks of heavy metals in Daya Bay, South China sea. Environmental Pollution, **382**, 126768, **2025**.
23. ZHANG H., WU J., LI Q., JIN M. A~300-year record of environmental changes in Lake Issyk-Kul, Central Asia, inferred from lipid biomarkers in sediments. Limnologica, **90**, 125909, **2021**.
24. CARVALHO A.C.B., MOREIRA V.A., VICENTE M.C., BIDONE E.D., BERNARDES M.C., SABADINI-SANTOS E. Sterol and PAHs fingerprint analysis of organic matter at Southeast Brazilian Bay. Marine Pollution Bulletin, **181**, 113899, **2022**.
25. DING Q., HUANG X., HU H., HONG M., ZHANG D., WANG K. Impact of pyrene and cadmium co-contamination on prokaryotic community in coastal sediment microcosms. Chemosphere, **188**, 320, **2017**.
26. VAN METRE P.C., MAHLER B.J., FURLONG E.T. Urban Sprawl Leaves Its PAH Signature. Environmental Science & Technology, **34** (19), 4064, **2000**.
27. ROSE N.L., ROSE C.L., BOYLE J.F., APPLEBY P.G. Lake-Sediment Evidence for Local and Remote Sources of Atmospherically Deposited Pollutants on Svalbard. Journal of Paleolimnology, **31** (4), 499, **2004**.
28. RAVINDRA K., SOKHI R., VAN GRIEKEN R. Atmospheric polycyclic aromatic hydrocarbons: Source attribution, emission factors and regulation. Atmospheric Environment, **42** (13), 2895, **2008**.
29. ADNAN N.H., ZAKARIA M.P., JUAHIR H., ALI M.M. Faecal sterols as sewage markers in the Langat River, Malaysia: Integration of biomarker and multivariate statistical approaches. Journal of Environmental Sciences, **24** (9), 1600, **2012**.
30. ELHADJ Z., BRAHIM-TAZI N.A., BELGUERMI A., HADDAD F.Z., BEKKAY Y., MEGHABAR R. Organic

and heavy metal pollutants in dredged sediment of Oran Harbor, Algeria. Environmental Monitoring and Assessment, **196** (9), 834, **2024**.
31. ARMIENTO G., BARSANTI M., CAPRIOLI R., CHIAVARINI S., CONTE F., CROVATO C., DE CASSAN M., DELBONO I., MONTEREALI M.R., NARDI E., PARRELLA L., PEZZA M., PROPOSITO M., RIMAURO J., SCHIRONE A., SPAZIANI F. Heavy metal background levels and pollution temporal trend assessment within the marine sediments facing a brownfield area (Gulf of Pozzuoli, Southern Italy). Environmental Monitoring and Assessment, **194** (11), 814, **2022**.
32. CORMINBOEUF A., MONTERO-SERRANO J.-C., ST-LOUIS R., DALPÉ A., GÉLINAS Y. Pre- and post-industrial levels of polycyclic aromatic hydrocarbons in sediments from the Estuary and Gulf of St. Lawrence (eastern Canada). Marine Pollution Bulletin, **174**, 113219, **2022**.
33. KIM M., HWANG J., MONTLUÇON D.B., HAGHIPOUR N., KIM D., KIM H.J., CHOI K.Y., KIM C.J., KANG C.-K., KIM Y.-I., EGLINTON T.I. Spatiotemporal variation of sterols in sediment as markers of primary production and ocean sewage dumping in the southwestern East Sea (Japan Sea). Marine Pollution Bulletin, **205**, 116680, **2024**.
34. RICHARD E.C., HAMACHER C., FARIAS C.O., DORE M.P., RIBEIRO N.C.M., PASSOS M.A., MARTINHO P.F., GODOY J.M., CARREIRA R.S. Historical Evolution of Organic Matter Accumulation in a Coastal Bay in the SW Atlantic, Brazil: Use of Sterols and n-Alcohols as Molecular Markers. Journal of the Brazilian Chemical Society, **25** (8), **2014**.
35. LIU X., CHENG P., ZHOU J., FAN Y., FU Y., TAN L., LAN J., ZHANG L., GU H., BI Y. Microplastic Characteristics in Equus kiang (Tibetan Wild Ass) Feces and Soil on the Southern Tibetan Plateau, China. Environmental Science & Technology, **57** (26), 9732, **2023**.
36. ZHANG X., SUN T., LI F., JI C., WU H. Risk assessment of trace metals and polycyclic aromatic hydrocarbons in seawater of typical bays in the Bohai Sea. Marine Pollution Bulletin, **200**, 116030, **2024**.
37. ZHANG R., ZHOU L., ZHANG F., DING Y., GAO J., CHEN J., YAN H., SHAO W. Heavy metal pollution and assessment in the tidal flat sediments of Haizhou Bay, China. Marine Pollution Bulletin, **74** (1), 403, **2013**.
38. ZHENG J.P., WANG C.Y., ZHAO Y.G., PENG M., WEI A.H. Distribution characteristics and potential risks of major pollutants in sediments from the Haizhou Bay fishing port economic zone and adjacent waters, China. Marine Environmental Science, **41** (5), 731, **2022** [In Chinese].
39. CAO S.N., LI J.K., CHEN L., XU Z.D., ZHU H.R., WANG J., YAO Z.Y. Seasonal variation, source apportionment, and health risk assessment of polycyclic aromatic hydrocarbons (PAHs) in $PM_{2.5}$ in Lianyungang City during 2019–2023. Public Health and Preventive Medicine, **36** (1), 65, **2025** [In Chinese].
40. DU J.J., MAO L.J., JIA Y.F., TAN Z.H., LI N., SUN Z.X. Geochemical characteristics and source identification of elements in sediments from the core in the Haizhou Bay. Marine Science Bulletin, **36** (4), 449, **2017** [In Chinese].
41. SHI W., XU M., LIU Q., XIE S. Polycyclic aromatic hydrocarbons in seawater, surface sediment, and marine organisms of Haizhou Bay in Yellow Sea, China: Distribution, source apportionment, and health risk assessment. Marine Pollution Bulletin, **174**, 113280, **2022**.
42. ZHANG S., FU K., GAO S., LIANG B., LU J., FU G. Bioaccumulation of Heavy Metals in the Water, Sediment, and Organisms from The Sea Ranching Areas of Haizhou Bay in China. Water, **15** (12), 2218, **2023**.
43. LIANYUNGANG MUNICIPAL BUREAU OF STATISTICS. Lianyungang Statistical Yearbook 2012. China Statistics Press, Beijing, **2012** [In Chinese].
44. LIU N., ZHANG D., CEN K., CUI L., LI J., LIU Q., LU J., LIN X. Influence of anthropogenic activities on the temporal and spatial variation of polycyclic aromatic hydrocarbons in the sediments of Jiangsu coastal zone, China. Continental Shelf Research, **170**, 11, **2018**.
45. HAN B., LIN F., DING Y., ZHENG L. Distribution characteristics, sources, and ecological risk assessment of polycyclic aromatic hydrocarbons in sediments from Haizhou Bay, China. Human and Ecological Risk Assessment: An International Journal, **24** (3), 847, **2018**.
46. JIANGSU PROVINCIAL DEPARTMENT OF ECOLOGY AND ENVIRONMENT. Bulletin on Ecological Environment Status of Jiangsu Province (2020). Jiangsu Provincial Department of Ecology and Environment, Nanjing, China, **2021** [In Chinese].
47. DU J.J., MAO L.J., TAN Z.H., GAO F., LI N. Pollution evaluation and source identification of heavy metals in sediments from core in Haizhou Bay, China. Marine Environmental Science, **35** (6), 814, **2016** [In Chinese]. AGENCY U.S.E.P. SW-846 Test Method 3630C: Silica Gel Cleanup. United States Environmental Protection Agency, Washington, D.C., **1996** [In Chinese].
48. AGENCY U.S.E.P. SW-846 Test Method 3630C: Silica Gel Cleanup. United States Environmental Protection Agency, Washington, D.C., **1996**.
49. BATTISTEL D., PIAZZA R., ARGIRIADIS E., MARCHIORI E., RADAELLI M., BARBANTE C. GC-MS method for determining faecal sterols as biomarkers of human and pastoral animal presence in freshwater sediments. Analytical and Bioanalytical Chemistry, **407**, 8505, **2015**.
50. LIU L.-Y., WANG J.-Z., WEI G.-L., GUAN Y.-F., ZENG E.Y. Polycyclic aromatic hydrocarbons (PAHs) in continental shelf sediment of China: Implications for anthropogenic influences on coastal marine environment. Environmental Pollution, **167**, 155, **2012**.
51. PAN C., CHEN K., CHEN D. Effect of Organics on Heavy Metal-Contaminated River Sediment Treated with Electro-Osmosis and Solidification/Stabilization Methods. Materials, **13** (6), 1466, **2020**.
52. TAN L., LIU Y., REN J. S., ZHANG J. The sources and burial fluxes of sedimentary organic carbon from the intensive mariculture zone in Haizhou Bay, China. Marine Pollution Bulletin, **218**, 118168, **2025**.
53. WANG N., GAO Q., CHENG H., WANG J. Heavy metals distribution and their ecological risk in the surface sediments of Haizhou Bay, China. Regional Studies in Marine Science, **78**, 103772, **2024**.
54. WU R. Determination of polycyclic aromatic hydrocarbon in atmospheric aerosol particle using capillary with gas chromatography-mass spectrometry. Mass Spectrometry, **1** (1), 3, **1981** [In Chinese].
55. LEI B.-H., XU M., CHEN J.-W., LIANG J., ZHANG Y.-G. Structural characteristics and evolution of the South Yellow Sea Basin since Indosinian. China Geology, **1** (4), 466, **2018**.
56. ZHANG J.M., WANG Z.C., FU J.D., WANG D.L., XIA N., WANG K., XU H.T., WANG L. Researches on activities

of main faults in Lianyungang City. Marine Geology & Quaternary Geology, **45** (2), 98, **2025** [In Chinese].
57. HOU D., CHENG X., WEI L., LI Y., LI K., ZHANG Z., ZHANG H., BIAN J., LI Y., SI W., JIA Z., HE J., HUANG Q. Oil and natural gas geochemistry in offshore China: Advances and challenges. Natural Gas Industry B, **11** (6), 631, **2024**.
58. YUAN Y., LI Q., CHEN J., CAO K., WANG J., ZHAO H., LAN T., ZHANG P., LUO D. Evaluation of the Suitability of China's Offshore Basins for CO2 Geological Storage. Journal of Ocean University of China, **24** (6), 1545, **2025**.
59. NOTAR M., LESKOVŠEK H., FAGANELI J. Composition, Distribution and Sources of Polycyclic Aromatic Hydrocarbons in Sediments of the Gulf of Trieste, Northern Adriatic Sea. Marine Pollution Bulletin, **42** (1), 36, **2001**.
60. LIMA A.L.C., FARRINGTON J.W., REDDY C.M. Combustion-Derived Polycyclic Aromatic Hydrocarbons in the Environment – A Review. Environmental Forensics, **6** (2), 109, **2005**.
61. GUO F., GAO M., DONG J., SUN J., HOU G., LIU S., DU X., YANG S., LIU J., HUANG Y. The first high resolution PAH record of industrialization over the past 200 years in Liaodong Bay, northeastern China. Water Research, **224**, 119103, **2022**.
62. HERSBACH H., BELL B., BERRISFORD P., HIRAHARA S., HORáNYI A., MUÑOZ-SABATER J., NICOLAS J., PEUBEY C., RADU R., SCHEPERS D., SIMMONS A., SOCI C., ABDALLA S., ABELLAN X., BALSAMO G., BECHTOLD P., BIAVATI G., BIDLOT J.-R., BONAVITA M., CHIARA G.D., DAHLGREN P., DEE D. The ERA5 global reanalysis. Quarterly Journal of the Royal Meteorological Society, **146** (730), 1999, **2020**.
63. FENG Z., WANG C., ZHANG C., WANG W., WANG J., LI Y., ZOU X. Air-Water Exchange and Gas-Particle Partitioning of Polycyclic Aromatic Hydrocarbons (PAHs) in Coral Reef Areas of the South China Sea. Journal of Geophysical Research: Atmospheres, **126** (9), **2021**.
64. DU J.J., MAO L.J., ZHANG R., DING Y.F., ZHU X.Q., WANG M.Q. Grain-size characteristics of tidal-flat core sediments in Haizhou Bay and their environmental implications. Bulletin of Marine and Lake Sciences, **1**, 88, **2016** [In Chinese].
65. LIU J., JIA J., GRATHWOHL P. Dilution of concentrations of PAHs from atmospheric particles, bulk deposition to soil: a review. Environmental Geochemistry and Health, **44** (12), 4219, **2022**.
66. SIUDEK P. Atmospheric Deposition of Polycyclic Aromatic Hydrocarbons (PAHs) in the Coastal Urban Environment of Poland: Sources and Transport Patterns, International Journal of Environmental Research and Public Health, **19** (21), 14183, **2022**.
67. MUDGE S.M., SEGUEL C.G. Organic Contamination of San Vicente Bay, Chile. Marine Pollution Bulletin, **38** (11), 1011, **1999**.
68. ISOBE K.O., TARAO M., ZAKARIA M.P., CHIEM N.H., MINH L.Y., TAKADA H. Quantitative Application of Fecal Sterols Using Gas Chromatography−Mass Spectrometry To Investigate Fecal Pollution in Tropical Waters: Western Malaysia and Mekong Delta, Vietnam. Environmental Science & Technology, **36** (21), 4497, **2002**.
69. RADA J.P.A., DUARTE A.C., PATO P., CACHADA A., CARREIRA R.S. Sewage contamination of sediments from two Portuguese Atlantic coastal systems, revealed by fecal sterols. Marine Pollution Bulletin, **103** (1-2), 319, **2016**.
70. MATIĆ BUJAGIĆ I., GRUJIĆ S., JAUKOVIĆ Z., LAUŠEVIĆ M. Sterol ratios as a tool for sewage pollution assessment of river sediments in Serbia. Environmental Pollution, **213**, 76, **2016**.
71. ZHANG A., ZHAO S., WANG L., YANG X., ZHAO Q., FAN J., YUAN X. Polycyclic aromatic hydrocarbons (PAHs) in seawater and sediments from the northern Liaodong Bay, China. Marine Pollution Bulletin, **113** (1-2), 592, **2016**.
72. LI H., LAI Z., ZENG Y., GAO Y., YANG W., MAI Y., WANG C. Occurrence, source identification, and ecological risk assessment of polycyclic aromatic hydrocarbons in sediments of the Pearl River Delta, China. Marine Pollution Bulletin, **170**, 170112666, **2021**.
73. LI S., TAO Y., YAO S., XUE B. Distribution, sources, and risks of polycyclic aromatic hydrocarbons in the surface sediments from 28 lakes in the middle and lower reaches of the Yangtze River region, China. Environmental Science and Pollution Research, **23** (5), 4812, **2016**.
74. QI X., GUAN K., LUO X., LU Q., HUANG C., ZENG Y., MAI B., WANG S. Distribution, source, and ecological risks of polycyclic aromatic hydrocarbons in surface sediments from contaminated urban rivers across China. Journal of Soils and Sediments, **24** (5), 2088, **2024**.
75. WANG C., WANG W., HE S., DU J., SUN Z. Sources and distribution of aliphatic and polycyclic aromatic hydrocarbons in Yellow River Delta Nature Reserve, China. Applied Geochemistry, **26** (8), 1330, **2011**.
76. GUIGUE C., TEDETTI M., DANG D.H., MULLOT J.-U., GARNIER C., GOUTX M. Remobilization of polycyclic aromatic hydrocarbons and organic matter in seawater during sediment resuspension experiments from a polluted coastal environment: Insights from Toulon Bay (France). Environmental Pollution, **229**, 627, **2017**.
77. HARTMANN P.C., QUINN J.G., CAIRNS R.W., KING J.W. The distribution and sources of polycyclic aromatic hydrocarbons in Narragansett Bay surface sediments. Marine Pollution Bulletin, **48** (3-4), 351, **2004**.
78. RAJPARA R.K., DUDHAGARA D.R., BHATT J.K., GOSAI H.B., DAVE B.P. Polycyclic aromatic hydrocarbons (PAHs) at the Gulf of Kutch, Gujarat, India: Occurrence, source apportionment, and toxicity of PAHs as an emerging issue. Marine Pollution Bulletin, **119** (2), 231, **2017**.
79. ARAÚJO M.P., HAMACHER C., FARIAS C.O., SOARES M.L.G. Fecal sterols as sewage contamination indicators in Brazilian mangroves. Marine Pollution Bulletin, **165**, 112149, **2021**.
80. LIEBEZEIT G., WÖSTMANN R. Coprostanol in Siak River sediments, E Sumatra, Indonesia. Bull Environ Contam Toxicol, **85** (6), 585, **2010**.
81. SHAH V.G., HUGH DUNSTAN R., GEARY P.M., COOMBES P., ROBERTS T.K., VON NAGY-FELSOBUKI E. Evaluating potential applications of faecal sterols in distinguishing sources of faecal contamination from mixed faecal samples. Water Research, **41** (16), 3691, **2007**.
82. BI S., YANG Y., XU C., ZHANG Y., ZHANG X., ZHANG X. Distribution of heavy metals and environmental assessment of surface sediment of typical estuaries in eastern China. Marine Pollution Bulletin, **121** (1-2), 357, **2017**.
83. SHEN H., HUANG Y., WANG R., ZHU D., LI W., SHEN G., WANG B., ZHANG Y., CHEN Y., LU Y.,

CHEN H., LI T., SUN K., LI B., LIU W., LIU J., TAO S. Global Atmospheric Emissions of Polycyclic Aromatic Hydrocarbons from 1960 to 2008 and Future Predictions. Environmental Science & Technology, **47** (12), 6415, **2013**.
84. LU Y., PHILP R.P., BIACHE C. Assessment of Fecal Contamination in Oklahoma Water Systems through the Use of Sterol Fingerprints. Environments, **3** (4), 28, **2016**.
85. ZHANG R., ZHANG F., ZHANG T.-C. Sedimentary records of PAHs in a sediment core from tidal flat of Haizhou Bay, China. Science of The Total Environment, **450-451**, 280, **2013**.
86. LI Y., WANG G., WANG J., JIA Z., ZHOU Y., WANG C., LI Y., ZHOU S. Determination of influencing factors on historical concentration variations of PAHs in West Taihu Lake, China. Environmental Pollution, **249**, 573, **2019**.
87. HE D., ZHANG K., TANG J., CUI X., SUN Y. Using fecal sterols to assess dynamics of sewage input in sediments along a human-impacted river-estuary system in eastern China. Science of The Total Environment, **636**, 787, **2018**.
88. LIN F., LI Y., LIN L., YUAN K., YANG L., HUANG Y., CHEN B., LUAN T. Spatiotemporal variations of halogenated polycyclic aromatic hydrocarbons in sediments of Pearl River Estuary: Occurrence, sources, and potential ecological risks. Marine Pollution Bulletin, **222**, 118722, **2026**.
89. COUNTWAY R.E., DICKHUT R.M., CANUEL E.A. Polycyclic aromatic hydrocarbon (PAH) distributions and associations with organic matter in surface waters of the York River, VA Estuary. Organic Geochemistry, **34** (2), 209, **2003**.
90. WANG Q., XU H., YIN J., DU S., LIU C., LI J.-Y. Significance of the great protection of the Yangtze River: Riverine input contributes primarily to the presence of PAHs and HMs in its estuary and the adjacent sea. Marine Pollution Bulletin, **186**, 114366, **2023**.
91. CHI Y., WANG J., BI J., LIU T., HUANG M., LI G., MA Y., ZHANG B.-T. Heavy Metals in Sediments of the Yangtze River, Poyang Lake and Its Tributaries: Spatial Distribution, Relationship Analysis and Source Apportionment. Water, **17** (9), 1295, **2025**.
92. ABDEL-SHAFY H.I., MANSOUR M.S.M. A review on polycyclic aromatic hydrocarbons: Source, environmental impact, effect on human health and remediation. Egyptian Journal of Petroleum, **25** (1), 107, **2016**.
93. LIN T., HU L., GUO Z., QIN Y., YANG Z., ZHANG G., ZHENG M. Sources of polycyclic aromatic hydrocarbons to sediments of the Bohai and Yellow Seas in East Asia. Journal of Geophysical Research: Atmospheres, **116** (D23), **2011**.
94. KATSOYIANNIS A., SWEETMAN A.J., JONES K.C. PAH molecular diagnostic ratios applied to atmospheric sources: a critical evaluation using two decades of source inventory and air concentration data from the UK. Environmental Science & Technology, **45** (20), 8897, **2011**.
95. BARTLETT M.S. Tests of significance in factor analysis. British Journal of Statistical Psychology, **3** (2), 77, **1950**.
96. KAISER H.F. An Index of Factorial Simplicity. Psychometrika, **39** (1), 31, **1974**.
97. DUODU G.O., OGOGO K.N., MUMMULLAGE S., HARDEN F., GOONETILLEKE A., AYOKO G.A. Source apportionment and risk assessment of PAHs in Brisbane River sediment, Australia. Ecological Indicators, **73**, 784, **2017**.
98. RAJEEV P., SHUKLA P.C., SINGH G.K., DAS D., GUPTA T. Assessment of entrainment of key PAHs emanating from major combustion sources into the ambient air. Fuel, **347**, 128430, **2023**.
99. ZHAO B., CHEN G., QIN L., HAN Y., ZHANG Q., CHEN W., HAN J. Effect of coal blending on arsenic and fine particles emission during coal combustion. Journal of Cleaner Production, **311**, 127645, **2021**.
100. MELLO T.J., LONGHINI C.M., WANDERLEY B.M.S., SILVA C.A.D., LEHRBACK B.D.C., BOM F.C., NETO R.R., SÁ F., VIEIRA E.A., COSTA V.E., LONGO G.O. Pollution affects even oceanic marine protected areas in Southwestern Atlantic. Environmental Pollution, **366**, 125485, **2025**.
101. PENG X., ZHANG G., MAI B., HU J., LI K., WANG Z. Tracing anthropogenic contamination in the Pearl River estuarine and marine environment of South China Sea using sterols and other organic molecular markers. Marine Pollution Bulletin, **50** (8), 856, **2005**.
102. HAN Y., ZHISHENG A., LEI D., ZHOU W., ZHANG L., ZHAO X., YAN D., ARIMOTO R., ROSE N.L., ROBERTS S.L., LI L., TANG Y., LIU X., FU X., SCHNEIDER T., HOU X., LAN J., TAN L., LIU X., HU J., CAO Y., LIU W., WU F., WANG T., QIANG X., CHEN N., CHENG P., HAO Y., WANG Q., CHU G., GUO M., HAN M., TAN Z., WEI C., DUSEK U. The Sihailongwan Maar Lake, northeastern China as a candidate Global boundary Stratotype Section and Point for the Anthropocene series. The Anthropocene Review, **10** (1), 177, **2023**.
103. ZHAO Y., WANG S., DUAN L., LEI Y., CAO P., HAO J. Primary air pollutant emissions of coal-fired power plants in China: Current status and future prediction. Atmospheric Environment, **42** (36), 8442, **2008**.
104. ZHANG R., ZHU G. A Review of the Research on Agricultural Technology Promotion in Modern Jiangsu. Ancient and Modern Agriculture, (4), 105, **2023** [In Chinese].
105. LI Z., FAN L., WANG L., MA H., HU Y., JIANG Y., AN C., LIU A., HAN J., JIN H. PAH Profiles of Emitted Ashes from Indoor Biomass Burning across the Beijing-Tianjin-Hebei Region and Implications on Source Identification. Aerosol and Air Quality Research, **18** (3), 749, **2018**.
106. LI Q. A Study on the Development of Modern Animal Husbandry in China. Doctoral Dissertation, Nanjing Agricultural University, **2003** [In Chinese].
107. LLIN Y.N., JIN X.B., YANG X.H., LONG Y., ZHOU Y.K. Estimation and spatial reconstruction of urban and rural construction land in Jiangsu Province in the last two hundred years. Acta Geographica Sinica, **72** (3), 488, **2017** [In Chinese].
108. DENG X., MAO L., WU Y., TAN Z., FENG W., ZHANG Y. Pollution, risks, and sources of heavy metals in sediments from the urban rivers flowing into Haizhou Bay, China. Environmental Science and Pollution Research, **29** (25), 38054, **2022**.
109. SUN X., DONG Z., ZHANG W., SUN X., HOU C., LIU Y., ZHANG C., WANG L., WANG Y., ZHAO J., CHEN L. Seasonal and spatial variations in nutrients under the influence of natural and anthropogenic factors in coastal waters of the northern Yellow Sea, China. Marine Pollution Bulletin, **175**, 113171, **2022**.
110. CHEN S., JIANG L., CHENG X., LIAO G., GERKEMA T. A Physical Perspective of Recurrent Water Quality Degradation: A Case Study in the Jiangsu Coastal

Waters, China. Journal of Geophysical Research: Oceans, **128** (8), e2022JC019607, **2023**.
111. EMBER Global Electricity Review 2023. Ember Climate, London, UK, **2023**.
112. ADMINISTRATION U.S.E.I. International Energy Outlook: China Electricity Indicators. U.S. Energy Information Administration, Washington, DC, USA, **2022**.
113. XU A., WU Y.-H., CHEN Z., WU G., WU Q., LING F., HUANG W.E., HU H.-Y. Towards the new era of wastewater treatment of China: Development history, current status, and future directions. Water Cycle, **1**, 80, **2020**.
114. ZHANG Q.H., YANG W.N., NGO H.H., GUO W.S., JIN P.K., DZAKPASU M., YANG S.J., WANG Q., WANG X.C., AO D. Current status of urban wastewater treatment plants in China. Environment International, **92-93**, 11, **2016**.
115. GUILHOT L. An analysis of China‘s energy policy from 1981 to 2020: Transitioning towards to a diversified and low-carbon energy system. Energy Policy, **162**, 112806, **2022**.